All Theses and Dissertations

2016-12-01

Facies Analysis and Depositional Environments of the Saints & Sinners Quarry in the Nugget Sandstone of Northeastern Utah

Jesse Dean Shumway
Brigham Young University

Follow this and additional works at: https://scholarsarchive.byu.edu/etd

Part of the Geology Commons

Facies Analysis and Depositional Environments of the Saints & Sinners Quarry in the Nugget

Sandstone of Northeastern Utah

Jesse Dean Scott Shumway

A thesis submitted to the faculty of
Brigham Young University
in partial fulfillment of the requirements for the degree of

Master of Science

Brooks B. Britt, Chair
Thomas H. Morris
Samuel M. Hudson

Department of Geological Sciences

Brigham Young University

ABSTRACT

Facies Analysis and Depositional Environments of the Saints & Sinners Quarry in the Nugget Sandstone of Northeastern Utah

Jesse Dean Scott Shumway
Department of Geology, BYU
Master of Science

The Saints & Sinners Quarry preserves the only known vertebrate body fossils in the Nugget Sandstone and the most diverse fauna known from the Nugget-Navajo-Aztec erg system. The fauna includes eight genera and >18,000 bone and bone fragments assignable to >76 individuals, including theropods, sphenosuchians, sphenodontians, drepanosaurs, procolophonids, and a dimorphodontid pterosaur. Cycadeoid fronds are the only plant fossils.

There are two depositional environments at the site – dune and interdune, each consisting of two or more faces. The dune facies are (1) Trough Cross-Stratified Sandstone (TCS) representing dry dunes, and (2) Massive and Bioturbated Dunes (MBD) representing bioturbated, damp dunes. The interdune facies are (1) Wavy Sandstone (WSS) representing wet and damp flats with biofilms and tridactyl tracks, (2) Green Clays and Silts (GCS) representing quiet lacustrine waters, (3) Planar Laminated Sandstone (PLS) representing lacustrine dust and sand storm deposits which grade laterally into (4) Massive Bone Bed (MBB) shoreline deposits.

The vertical and lateral relationships of the dune and interdune facies suggests that an interdune flat developed (WSS facies) likely by deflation of dunes down to, or near to, the water table. As the water table rose, a shallow lake developed (GCS facies) and trapped wind-blown sediment during sand storms (PLS Facies). The taxonomically diverse vertebrate fauna suggest a mass die-off occurred, likely due to drought. The carcasses and bones were buried by three distinct depositional events, each a bone bed (MBB facies) - separated by very thin clays (GCS facies). Thereafter the water table dropped resulting in several cm-scale sandstone beds with tridactyl tracks (WSS facies). Then migrating dunes buried the interdune flat. These dunes hosted burrowing invertebrates for a moderate time resulting in the destruction of nearly all primary sedimentary structures (MBD facies). Ultimately, as the area dried further, more dunes migrated over these bioturbated surfaces and the area returned to dune field conditions (TCS facies).

The Saints & Sinners site indicates that a previously unrecognized, remarkably diverse vertebrate fauna thrived in wet interdunes of western North America's Late Triassic erg system. A massive-die-off, likely due to a drought, provided a wealth of carcasses and their bones. The dynamic shoreline representing the interface of dunes and standing water provided favorable conditions for rapid burial of small carcasses and the disarticulated bones of larger individuals.

Keywords: interdune, eolian, facies analysis, depositional environments, Nugget Sandstone

ACKNOWLEDGEMENTS

TABLE OF CONTENTS

LIST OF TABLES AND FIGURES

INTRODUCTION

Since its discovery in 2008 (Britt et al., 2016) the Saints & Sinners dinosaur quarry in northeastern Utah has continued to surprise geologists and paleontologists yielding more than 18,000 bones. These bones include the only known vertebrate body fossils from the Nugget Sandstone. Not only do the strata preserve unique and spectacular body fossils, but it also preserves the most diverse fauna known from the Late Triassic to Middle Jurassic North American erg systems including the Navajo Sandstone, Aztec Sandstone, and Nugget Sandstone (Fig. 1A) (Chure et al., 2014; Rowland and Mercadante, 2014; Good and Ekdale, 2014; Wilkens et al., 2007; Irmis, 2005; Tykoski, 2005; Sues et al., 1994). The fauna preserved at Saints & Sinners includes nine genera represented by more than 76 individuals, including theropods, sphenosuchians, sphenodontians, a drepanosaur, a procolophonid, a pterosaur, and cycadeoid fronds (Table 1). A facies analysis of the quarry strata presented in this work indicates that interdunal lacustrine depositional environment contributed to the accumulation and preservation of this unprecedented fossil assemblage.
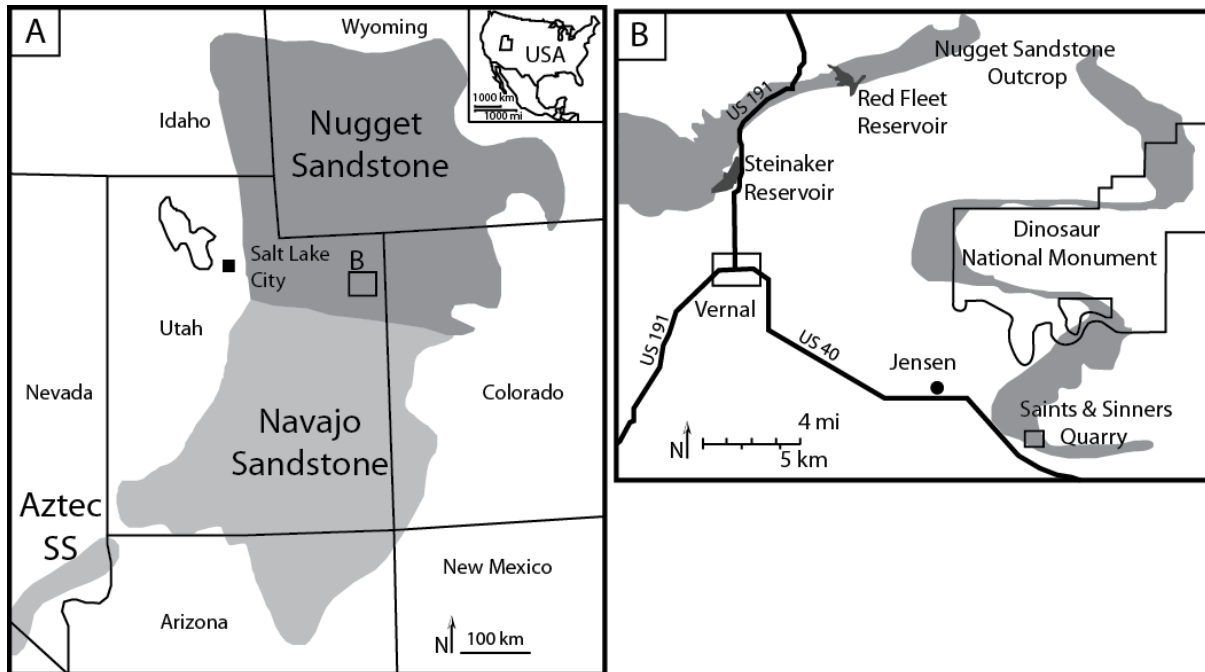
Figure 1 Location of western North American ergs and the Saints & Sinners Quarry. A) Relative positions of select Late Triassic to Middle Jurassic eolian formations. B) Outcrops of the Nugget Sandstone near Vernal, Utah in grey and location of Saints & Sinners Quarry between Jensen, Utah and Utah – Colorado border. Exact location of the quarry is on file with the BYU Museum of Paleontology as locality 1442 and with the BLM as UT08-025E. Map A modified from Good (2013) and map B modified from Good and Ekdale (2014).

Purpose and Scope

This paper presents the latest data and interpretations concerning the depositional environment and depositional history of the Saints & Sinners Quarry. It also addresses the spatial extent of the depositional environment and implications for the Nugget Sandstone. Lastly, this paper lays a geologic framework for future taphonomy and paleontology studies of the site.

Table 1 Saints & Sinners Quarry faunal list

			Size, approx.	Common name	Notes	# Individuals
Body fossils		Plantae				
		Gymnospermophyta				
		Cycadeoidophyta	cycadeoid		Bennettitalian "cycad"	isolated frond, rhachi, petioles	
		Animalia				
		Sauroposida "Reptilia"				
		Anapsida				
		Procolophonidae	*Leptopleuron*-like	22 cm long	parareptilian	isolated dentaries	3
		Diapsida				
		incerta sedis	drepanosaurid	40 cm long	bird-like head, digging arms	articulated, associated, disarticulated	>5
		Lepidosauromorpha	sphenodontian A, normal-jawed	30 cm long	tuatara-like "lizard"	isolated jaw elements	1
		Lepidosauromorpha	sphenodontian B, slender-jawed	30 cm long	tuatara-like "lizard"	isolated jaw elements	3
		Crocodylomorpha	sphenosuchian A, primitive	20 to 50 cm long	crocodylomorph, terrestrial	articulated, associated, disarticulated	>41
		Crocodylomorpha	sphenosuchian B, large	~1.5 m long	crocodylomorph, terrestrial	braincase, dermal ossicles	1
		Pterosauria	dimorphodontid	1.5 m wingspan	pterosaur	single individual, partial skull + phalanx	1
		Dinosauria, Theropoda	coelophysoid	1.5 to 3 m long	predatory dinosaur	disarticulated	20
		Dinosauria, Theropoda	medium-sized theropod	7 m long	predatory dinosaur	teeth, partial vertebrae	1
Trace fossils		Invertebrata	*Skolithos*	< 8 mm diameter	invertebrate burrows	in dune facies	
			Planolites	< 8 mm diameter	invertebrate burrows	in dune facies	
		Vertebrata	*Grallator*	~15 cm long	small tridactyl tracks	on top of lacustrine & crinkly beds	
			burrow at toe of dune to beach	15 cm x 1.5 m	vertebrate burrow	single occurrence	

Geographic Context

The Saints & Sinners dinosaur quarry is located in northeastern Utah, just south of Dinosaur

National Monument (Fig. 1 and Fig. 2) on a cuesta of the Nugget Sandstone. Stratigraphically,

the quarry is located approximately 65 m above the base of the eolian, cliff-forming portion of the Nugget Sandstone (Fig. 3).

Figure 2 Saints & Sinners Quarry. Overview looking north (A) and down (B). Quarry location is indicated in each figure.
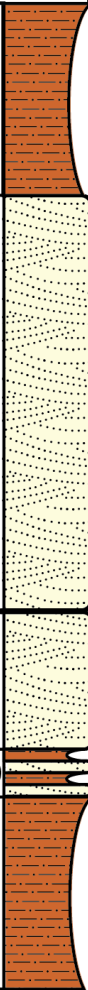
Period	Formation	Meters
JURASSIC	Carmel Formation	70 - 140
	Nugget Sandstone	150 - 260
_?_	Saints and Sinners Quarry	0-4
TRIASSIC		50
	Bell Springs Fm.	17 - 20
	Chinle Formation	70 - 140

Figure 3 Simplified regional stratigraphy. Modified from Hintze (1993).

The eolian sandstones of northeastern Utah where the Saints & Sinner Quarry is located have been studied for nearly 150 years and gone by several names. In 1876, Powell first called these sandstones along with the eolian sandstones of southern Utah the White Cliff Sandstone (Powell, 1876). The northern sandstones were renamed the Nugget Sandstone after the Nugget Station west of Kemmerer, Wyoming by Veatch in 1907 (Veatch, 1907). Over the next couple decades, geologists began calling the southern sandstones the Navajo Sandstone, while the northern sandstone continued to be referred to as the Nugget Sandstone.

During this same time, the Navajo Sandstone, Kayenta Formation, and Wingate Sandstone were determined to be a conformable package and named the Glen Canyon Group (Gregory and Moore, 1931; Kinney, 1955). In 1955, Kinney replaced the term Nugget Sandstone with Navajo Sandstone for the eolian sandstones in northeastern Utah on the south flank of the Uinta Mountains (Kinney, 1955). In 1964, Poole and Stewart (1964) used the term Glen Canyon Sandstone for the same rocks (Poole and Stewart, 1964). Later, High and Picard (1975) returned to the Wyoming nomenclature, and used Nugget Sandstone. Thus the eolian sandstones below the Carmel Formation of northeastern Utah have been called the White Cliff Sandstone, Nugget Sandstone, Navajo Sandstone, and Glen Canyon Sandstone.

	Southwest Utah			Southeast Utah			Northeast Utah
Jurassic	Carmel Formation			Carmel Formation			Carmel Formation
	Glen Canyon Group	Navajo SS		Glen Canyon Group	Navajo SS		Nugget Ss
		Kayenta Fm			Kayenta Fm		
		Moenave Fm			Wingate SS		
Triassic	Chinle Formation						Bell Springs Fm
				Chinle Formation			Chinle Formation
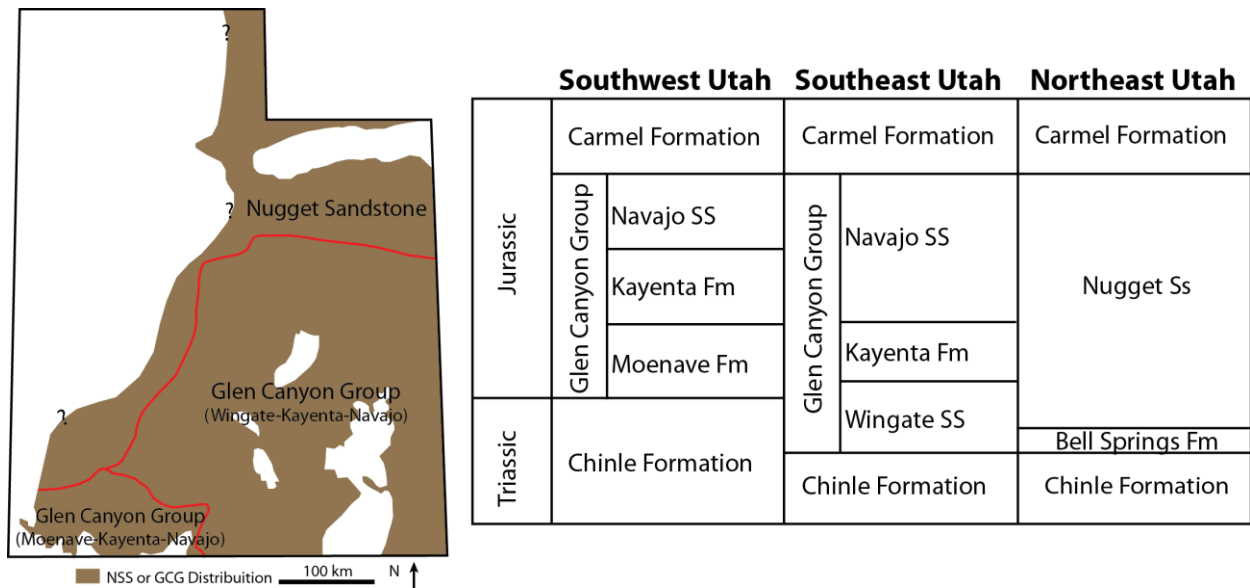
Figure 4 Distribution, nomenclature, and lateral equivalents of the Nugget Sandstone. Modified from Sprinkel (2011).

Sprinkel et al. (2011) conclude that the eolian sandstone unit below the Carmel Formation of northeastern Utah correlates with the Glen Canyon Group in southern Utah, which consists of (in ascending order) the Wingate Sandstone, Kayenta Formation, and Navajo Sandstone (Fig. 4). The authors surmise that the fluvial Kayenta Formation either pinches out or transitions to eolian deposition in northern Utah and that the Nugget Sandstone correlates specifically with the Wingate Sandstone and lower Navajo Sandstone. They further deduce that the term Nugget Sandstone should be used where the Kayenta Formation is not recognized and the term Glen Canyon Group should be used where they Kayenta Formation is recognized. The work presented in this paper will follow the nomenclature suggested by Sprinkel et al. (2011) and refers to the Upper Triassic to Lower Jurassic eolian sandstone of northeast Utah as the Nugget Sandstone.

The Nugget Sandstone caps the Upper Triassic trend of increasing aridity through time (Fig. 3) (Irmis et al., 2011). The oldest, stratigraphically lowest, and least arid formation in this trend, is the Upper Triassic Chinle Formation that outcrops in New Mexico, Arizona, Nevada, Utah, and Colorado (Stewart et al., 1972; Dubiel, 1994). It is interpreted as a mostly fluvial and overbank system with a minor lacustrine component. These sediments were deposited by large, low-gradient meandering systems that drained to the northwest (Blakey and Gubitosa, 1983; Dubiel, 1994; Riggs et al., 1996; Dickinson, 2004). Interfingering fluvial and overbank (Chinle Formation-like) sediments with eolian (Nugget Sandstone-like) sediments have been described as the Bell Springs Formation in northeastern Utah, the Bell Springs Member in Wyoming, and the Rock Point Formation in the Four Corners region (May, 2014). These transitional beds show an increase in aridity and a conformable change from the wet Chinle Formation to the more arid Bell Springs Formation (Irmis et al., 2015; May, 2014). The eolian Nugget Sandstone is conformable with the Bell Springs Formation (Sprinkel et al., 2011; May, 2014) and is the most arid of the Upper Triassic sediments (Blakey and Gubitosa, 1983; Riggs et al., 1996; Dubiel, 1994; Dickinson, 2004).

The Nugget Sandstone is the oldest formation of an expansive erg system that includes the Glen Canyon Group, and Aztec Formation (Fig. 1A) (Kocurek and Dott Jr., 1983; Sprinkel et al., 2011; Milligan, 2012). During deposition, this late Triassic to early Jurassic erg was larger than the present day Sahara with an estimated area of 1,370,000 km^2 (850,000 mi^2). Outcrops are located in present day Idaho, Wyoming, Colorado, Utah, Arizona, New Mexico, Nevada, and California (Kocurek and Dott Jr., 1983; Milligan, 2012; Good, 2013). The Nugget Sandstone is

characterized by tall (up to 9 m) sets of sweeping cross beds of fine to medium grained quartz sandstone. The Nugget Sandstone is interpreted to have been deposited in an arid climate with prevailing winds blowing from the north to the south (High Jr and Picard, 1975; Knapp, 1978; Doelger, 1987; Good, 2013; Irmis et al., 2015). Periodic humid or wet episodes deposited thinner, horizontal, and laterally continuous sandstone or carbonate beds (Loope and Rowe, 2003; Good, 2013) that become less abundant towards the top of the formation (Good, 2013).

Tectonic Setting

The Chinle Formation, Bell Springs Formation, and Nugget Sandstone were deposited in a retro-arc continental foreland basin along the western cratonic edge of North America (Blakey and Gubitosa, 1983). The basin is associated with Cordilleran Andean-type volcanic arcs to the west that originated in the early Mesozoic from eastward subduction. To the east of the basin were the remnants of the Ancestral Rockies uplift (Blakey and Gubitosa, 1983; Marzolf, 1988; Dickinson, 2004). Paleolatitude estimates put the basin somewhere between 20˚ and 30˚ north of the equator, and roughly in current global 30˚ trade winds belt of high-pressure (Loope et al., 2001; Kent and Irving, 2010). A northerly tectonic migration from the paleoequatorial to the high-pressure desert zone and/or the termination of monsoonal conditions associated with the break up of Pangaea likely contributed to the gradual desertification of the Late Triassic strata (Dubiel, 1994; Kent and Tauxe, 2005).

Nugget Sandstone Age

The Nugget Sandstone has been assigned a Triassic/Jurassic age because it is between the Late Triassic Chinle Formation, constrained by zircon U-Pb radiometric dates (Irmis et al., 2011) and

the Middle Jurassic Carmel Formation constrained by laser-fusion single-crystal $^{40}Ar/^{39}Ar$ measurements (Kowallis et al., 2001). Sprinkel (2011) noted that the Nugget Sandstone is the lateral equivalent of the Wingate and Navajo sandstones and the former contains the Triassic-Jurassic boundary. *Brachychirotherium* trackways (Lockley et al., 1992) near the base of the Nugget Sandstone were likely produced by the Late Triassic aetosaurs (Lucas and Heckert, 2011). Thus the base of the Nugget Sandstone is Late Triassic in age. The occurrence of drepanosaurs and procolophonids in the Saints & Sinners Quarry (Table 1) provide additional evidence of a Late Triassic age for the quarry horizon as drepanosaur are known only the Middle to Late Triassic (Renesto et al., 2009) and procolophonids range from the Permian to Late Triassic (Cisneros, 2008). Zircon grains from samples collected at the quarry as part of this study did not yield depositional ages. Previous zircon work indicates grains were derived from basement provenances older than 285 Ma in eastern and central Laurentia. The most prominent age populations reflect age derivation from Paleozoic, Neoproterozoic, and Grenvillian sources associated with the Appalachian orogen (Dickinson and Gehrels, 2009). Thus the Saints & Sinners fauna confirms that (1) at least the basal 65 meters of the Nugget Sandstone is Late Triassic in age, (2) the Triassic-Jurassic boundary is well above the base of the Nugget Sandstone, and (3) the lower half of the Nugget Sandstone is possibly time equivalent to part of the Wingate Sandstone.

METHODS

A synthesis of outcrop, thin section, photogrammetric model, XRD, and fauna data, were used to understand the depositional history of the Saints & Sinners Quarry.

Stratigraphic sections of outcrop were measured with a measuring tape, and field compass. Measuring focused on bone bearing sediments, and the strata immediately above and below. For each unit, the following descriptions were made: lithology, grain size, sorting, bedforms, sedimentary structures, thickness, variability, lateral continuity, cementation, fossil content, weathering, vertical extent, and Geological Society of America Rock-Color Chart color (Committee. and America., 1991). Pictures of outcrop were taken as necessary.

George Engelmann previously created twenty-five thin sections from various locations throughout the quarry. These thin sections, along with three others created for this study, provided a thin section of almost every stratigraphic unit described. Thin sections were made following normal vacuum and epoxy procedures at Wagner Petrographic. Visual mineralogical estimations, grain size, rounding, and sorting data were collected from the thin sections.

Two photogrammetric models based on drone-captures aerial photographs were created for this study. The first was created by Dr. Kevin Franke's team at BYU. Pete Kelsey's group at Autodesk created the second photogrammetric model of the quarry and surrounding outcrops. The latter model was analyzed using Autodesk Memento™ ("Momento"), Autodesk ReCap™ ("ReCap"), and Blender™ ("Blender") to better understand the facies' spatial relationships.

Samples of the Green Clays and Silts Facies were prepared for X-ray analysis according to specifications for analysis with RockJock11. RockJock11 calculates an XRD curve from selected mineral inputs and fits the calculated curve to the measured curve by varying the fraction of each mineral pattern until the degree of fit parameter between the measured and calculated curves is minimized. The results are presented as a list of minerals with their corresponding weight percent, and a calculated XRD curve with its degree of fit.

The sample preparation method for XRD analysis was developed by Omotoso and Eberl (2009) and is modified from Srodon and others (Srodon et al., 2001). First, the sample is passed through a 250µm sieve. Next, 1.0 g of sample, 0.25 g corundum, and 4 mL of ethanol are ground for 5 minutes in a McCrone micronizing mill. The mixture is then removed and left to dry overnight at 80˚ C. Once dried, the sample and corundum mixture is shaken in a plastic scintillation vial (20-25 mL) with 3 plastic balls (10 mm diameter) for 5 minutes. Then 0.5 mL hexane is added and the vial is shaken again for 10 minutes. The vial cap is removed and the sample left to dry under a hood for several minutes. Once dried, the powder is again passed through a 250 µm sieve and is ready to be loaded into an XRD sample holder (Eberl, 2003).

A standard steel sample holder was used with a 1.00 mm aluminum insert. Samples were analyzed in the BYU XRD lab using the PANalytical X'Pert Pro MPD diffractometer with a sealed tube Cu X-ray source and an X'Celerator detector. A Ge monochromator was used to provide a monochromatic source of the Cu Kα1 wavelength (1.5406 Å). Data collected from the defractometer was converted from the original 0.0167113 degree step size to a 0.02 degree step size using RockJock11 and then analyzed using RockJock11 to determine mineral composition.

FACIES DESCRIPTION

The Nugget Sandstone at Saints & Sinners Quarry consists of six distinct facies (Table 2). The facies are distinguished by sedimentological and diagenetic features observable in outcrop (Fig 5) and thin section. The facies will be discussed in two depositional groups: dune and interdune.

Table 2 Facies overview. Facies present at quarry with corresponding interpretation

Facies Acronym	Facies Name	Dominant Lithology	Features	Association	Interpretation
WSS	Wavy Sandstone	sandstone	wavy and wrinkly laminae; ridge structures; small TCS; ridge structures; trackways and footprints	interdune	damp to dry subaerial playa pan with strong algal mat growth
GCS	Green Claystone and Siltstone	siltstone	green clays silts	interdune	quiet standing water
PLS	Planar Laminated Sandstone	sandstone	planar laminated fine to very fine sands; common mm-cm thick silt/clay beds	interdune	wind storm sands deposited in lake
MBB	Massive Bone Bed sandstone	sandstone	massive bedded; relict ripple-like structures articulated to disarticulated skeletons; oriented and non-oriented bones	interdune	oasis shoreline
TCS	Trough Cross-Stratified Sandstone	sandstone	large to small trough cross-stratification	dune	dry eolian dunes
BMS	Burrowed and Massive Sandstone	sandstone	relict trough cross-stratification; massive sands; burrowed trough cross-stratification	dune	bioturbated eolian dunes with varying degrees of bioturbation
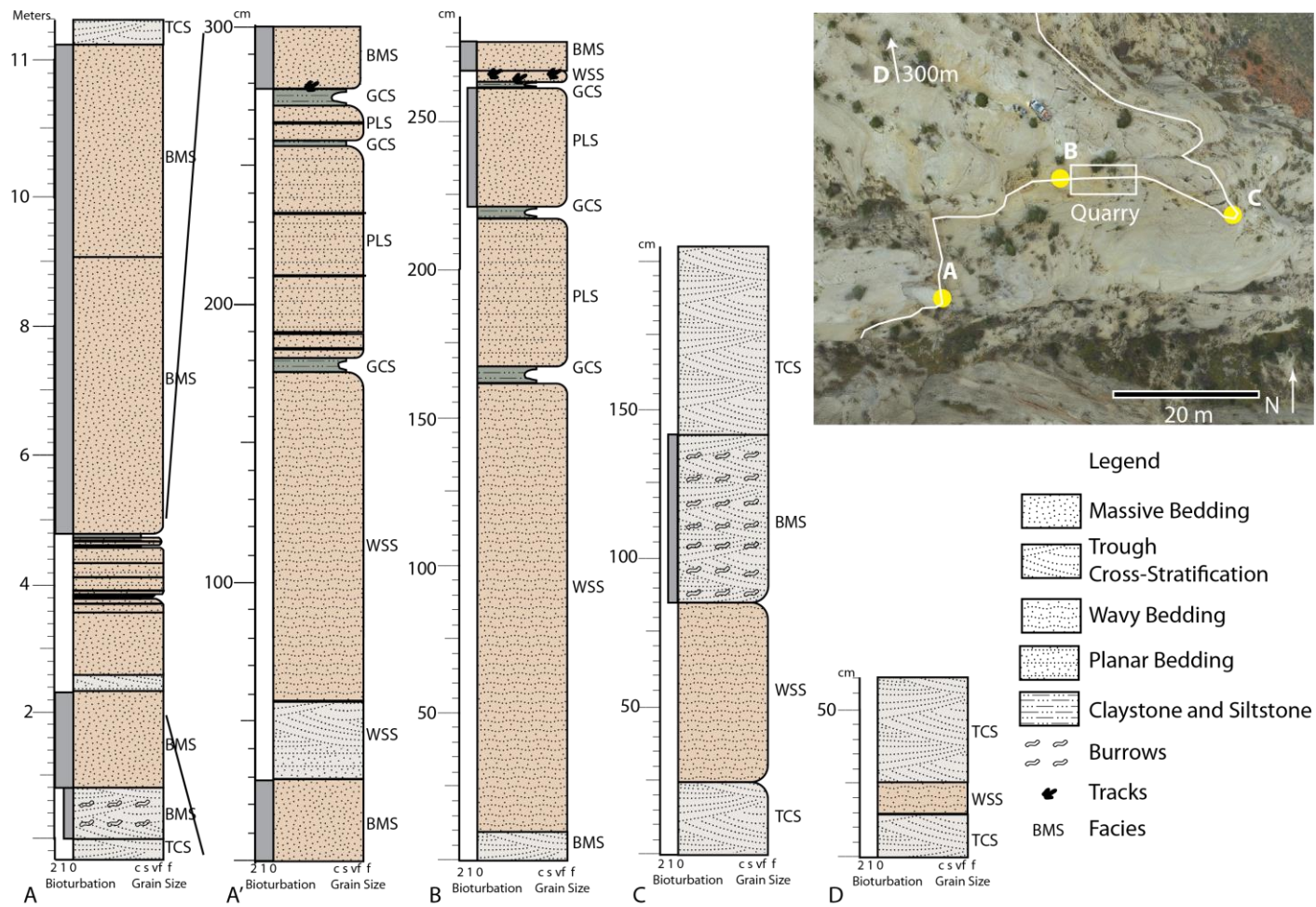
Figure 5 Stratigraphic sections. Four stratigraphic sections at Saints & Sinners Quarry. Letters A though D at bottom left of each column correslaketo locations indicated by yellow dots on the photogrammetric model in the upper right of the image. A' is an enlargement of the interdune facies in column A. Facies are indicated to the right of each unit. A white line on the model marks the interdune outcrop. The degree of bioturbation is indicated to the left of each unit with grey rectangles: scale 0 = none, 1 = moderate, 2 = high. Sediments plunge into the subsurface where the line ends southwest of stratigraphic column A.

14

Wavy Sandstone (WSS). In outcrop, this facies is white to very pale orange and predominantly ledge forming. It is easily distinguishable by the rust colored wavy iron laminae intercalated between wavy and wrinkly sands (Fig. 6B). Sedimentary structures include wavy, wrinkle (Fig. 6A), and flat laminations, trough cross-stratification (Fig. 6B), ridge structures (Fig. 6D) pillar structures, and massive bedding. Sedimentologically, the facies is made up of fine to very fine sand that is rounded to sub-rounded and well sorted.
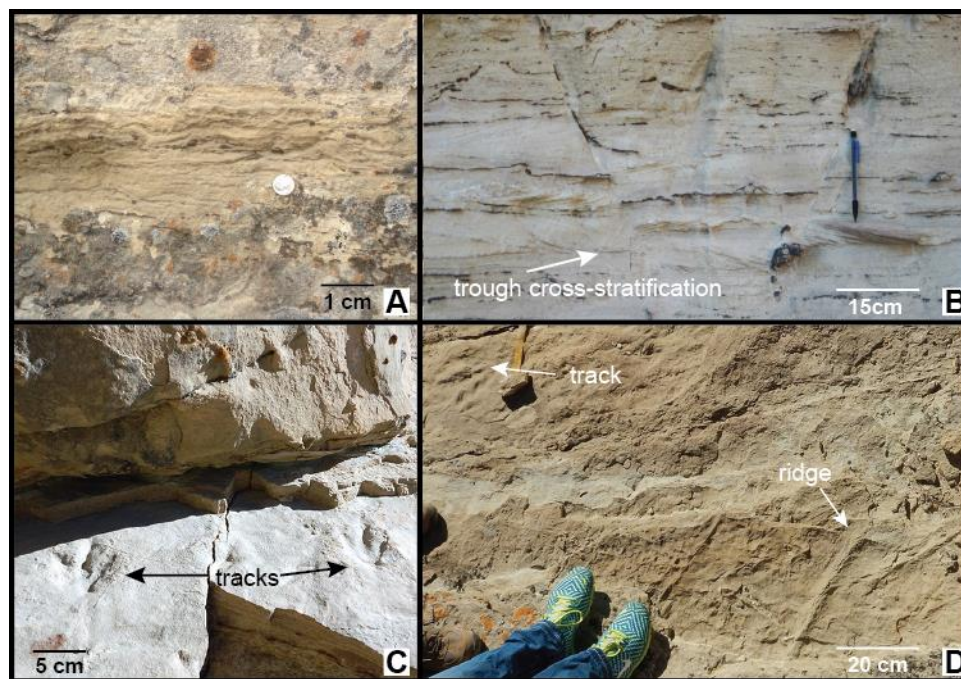
Figure 6 Wavy Sandstone facies. A) Wavy and wrinkly lamina at stratigraphic column D from Figure 2. B) Small cross-stratified beds near stratigraphic column A between wavy and wrinkly lamina highlighted by hematite cemented laminae. C) *Grallator* tracks in uppermost unit. D) Pressure ridge structures and a *Grallator* track.

The stratigraphically lowest unit of this facies is the most laterally extensive interdune bed and can be traced for 320 meters, almost ¼ of a mile, before the bed is truncated by faults. The facies ranges from 10 cm to 160 cm thick. The bed thins to the north and east of the quarry. To the west

and south of the quarry, the bed thickens slightly. At the thickest location (Fig. 5 point A) this bed shows a distinct succession of sedimentary structures. The bottom 6 to 9 cm contains wavy and wrinkly laminations with iron pinstripes. The next 15 to 20 cm is 3 to 4 trough-cross-stratified sets where each set is about 5 cm tall. Above the trough-cross-stratified sets is 100 cm of wavy lamination, pillar structures, and iron pinstripes, which gradually transition to massive sand in the top 20 cm. This succession is preserved along a 10 m tall outcrop wall. At other locations, this complete succession is not preserved, and wavy laminations, wrinkle laminations, and iron pinstripes characterize the facies.

The stratigraphically highest unit of this facies is the last occurrence of interdune sediments and contains wrinkle laminations, adhesion laminations, footprints, and ridge structures (Fig. 6C and 6D).

In thin section, this facies is more than 95 % quartz grains that are well sorted, rounded to sub-rounded, fine to very fine sand with calcite and opaque (iron) cement.

Green Claystone and Siltstone (GCS). In outcrop this facies is easily distinguishable by its greenish gray color. It is comprised predominantly of recessive siltstones and claystones, and has laminar shaley characteristics. The silts and clays are commonly interbedded with sometimes-undulatory beds and lenses of bluish white to yellowish gray very fine sandstone <1 to 5 cm thick. Wrinkled iron pinstripe beds (Fig. 7A) are also common. Most bed contacts are undulatory. Mudcracks are not present. Bed thickness ranges from 20 cm thick to <2mm thick at the quarry. Beds pinch out at the quarry and do not continue eastward.

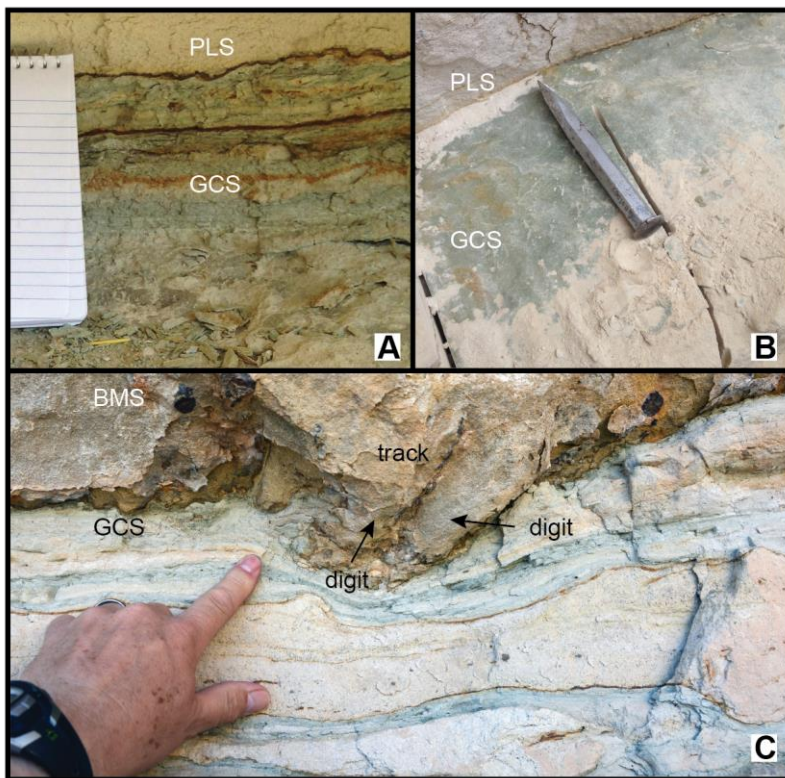**Figure 7 Green Clays and Silts facies.** A) cross section view B) plan view C) cross section view with the three toes of a tridactyl dinosaur track that deformed the underlying claystone and sandstone beds.

Based on thin sections, this facies consists of very poorly sorted quartz, clay, potassium feldspar and opaques. Quartz and clay are predominant, each ranging from 80% to 20% depending on

sample location. Potassium feldspar and opaques are less common. Grains are sub-rounded and range in size from coarse silt to clay size.

Planar Laminated Sandstone (PLS). This facies outcrops as a very pale orange ledge with sharp, sometime undulatory, basal contacts, bounded above and below by the Green Claystone and Siltstone Facies (Fig. 8B). Bedding consists of faint planar laminations (Fig. 8A). Sands in this facies are fine to very fine, sub-rounded, and moderately well sorted. Bed thickness ranges from 10 to 80 cm. All beds are located west of the quarry. Beds thin to the east and north, and grade into the massive bone bed facies immediately west of the quarry.

In thin section, this facies is more than 95% quartz grains that are moderately well sorted to well sorted, sub-rounded fine to very fine sand with calcite and iron cement.
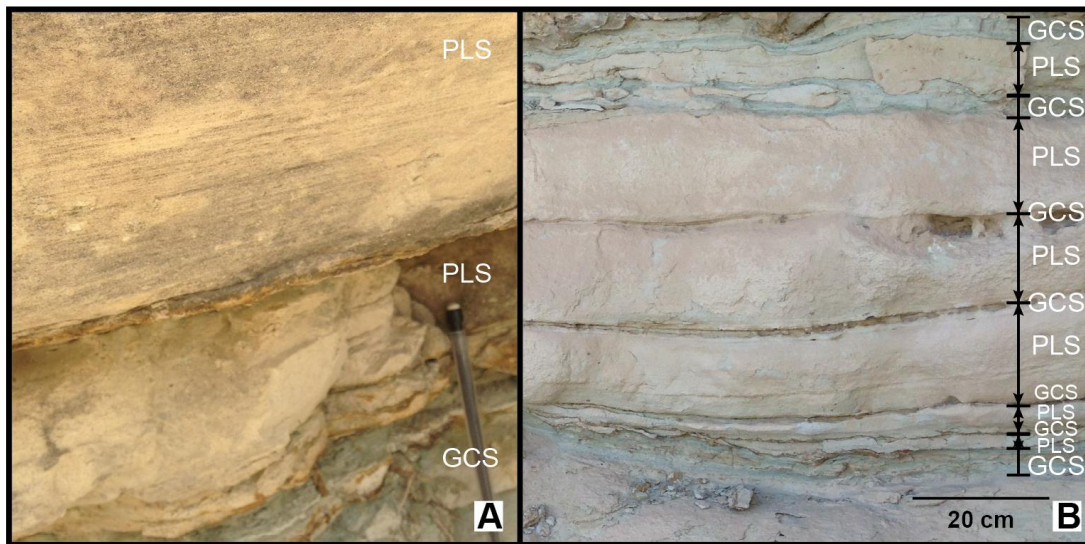

Figure 8 Planar Laminated Sandstone facies. A) Laminations in the PLS facies are faint. B) GCS facies above, below, and within the PLS facies.

Massive Bone Bed (MBB). This facies outcrops as very pale orange slopes and ledges. Sands grains are fine to very fine, moderately well sorted and sub-rounded. Bedding, for the most part, is massive with occasional wavy ripple-like structures (Fig. 9). This is the only facies that contains bones and the only quarried facies. To the west of the quarry, this facies grades into the Planar Laminated Sandstone facies. Beds of this facies pinch out immediately east of the quarry. Beds are bounded by sub-mm-thick beds of GCS facies.
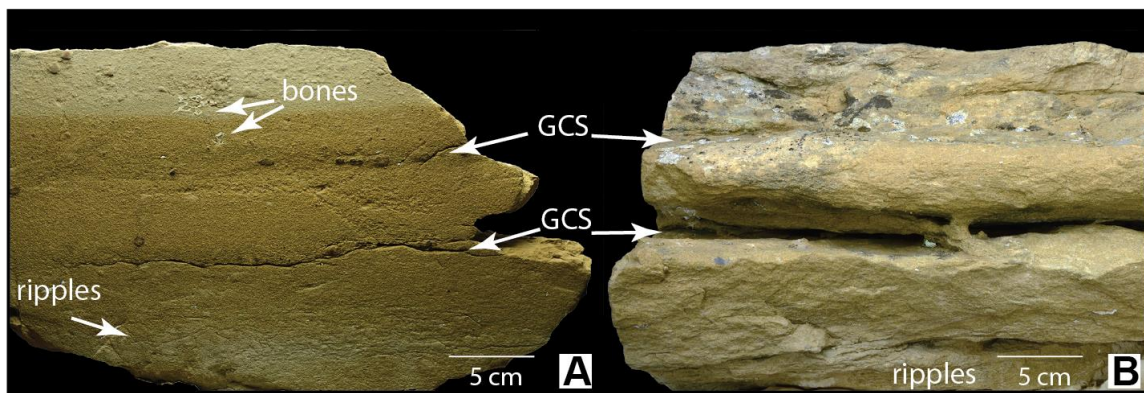
Figure 9 Massive Bone Bed facies. Two views of the same block of bone bed 2, an example of the massive bone bed facies. A) Cut cross section and B) weathered outcrop surface.

Bones are found in three distinct units separated by sub-mm-thick silt parting planes of the GCS facies (Fig. 10). Bone bed 1, the stratigraphically lowest unit averages 24 cm thick and contains sparse, small bones and articulated drepanosaurus and sphenodontian skeletons at the top of the unit. The skeletons of some individuals seem to span from the top of bone bed 1 into the bottom of bone bed 2, spanning the silty clay parting separating the two bone beds. Bone Bed 2, ranging from 20 to 30 cm thick, also has articulated skeletons at the base, above the GCS parting separating it from Bone Bed 1. Bone bed 2 has articulated skeletons of drepanosaurs and sphenodontians at least up the middle of the unit. The middle of the unit preserves a closely associated to partially articulated pterosaur skull and associated bones of coelophysoids. The

upper portion of the bone bed likewise contains associated but disarticulated bones to fully disarticulated bones of a variety of taxa (Fig. 9). Plant fossils are present on the underside of the silt parting plane separating bone bed 2 from bone bed 3. Bone bed 3, the stratigraphically highest bone bed, is 13 cm thick and contains disarticulated skeletons and preferentially oriented long bones.
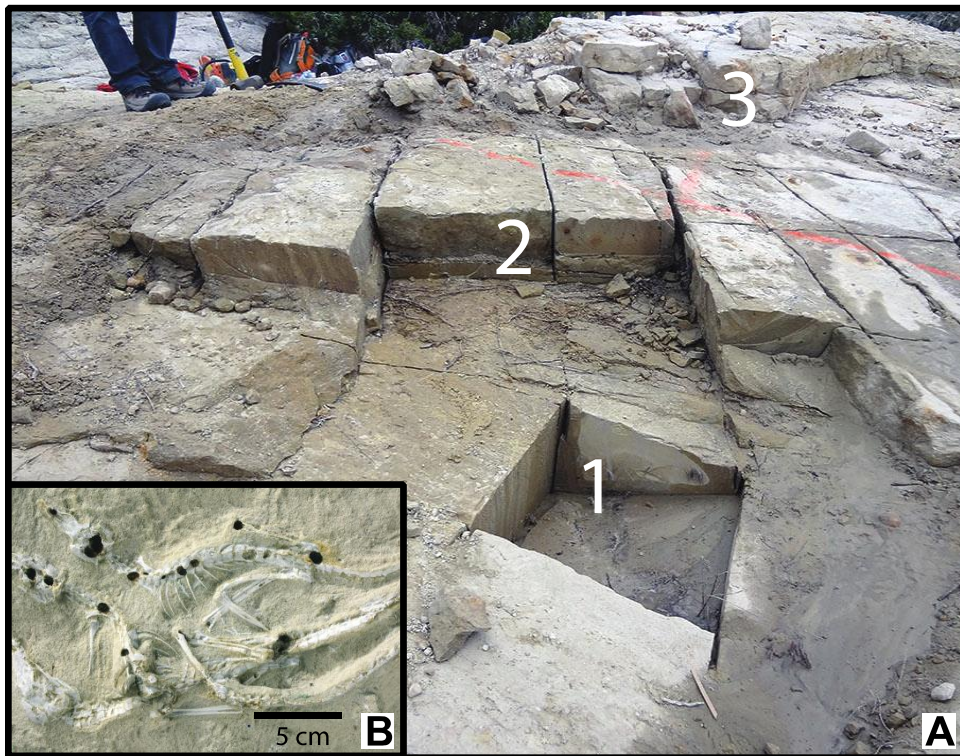
Figure 10 Bone beds. A) Three bone bed units of MBB facies each separated by sub-mm-thick beds of GCS facies. B) Three articulated sphenosuchians extracted from bone bed 2. The black pits are weathered and eroded concretions.

Trough Cross-Stratified Sandstones (TCS). This facies is by far the most common facies of the Nugget Sandstone. Locally, the facies outcrops as cliff-forming bluish white sandstone. It is characterized by large to small trough cross-stratification (Fig 11). Sand size ranges from very fine sand to fine sand that is well sorted and well rounded. Basal contacts are sharp. In thin section, this facies is more than 95% quartz grains that are well sorted, well rounded, fine to very fine sand with calcite cement.

Figure 11 Trough Cross-Stratified Sandstones. A) TCS facies to the 50 m to the north of, and stratigraphically above the quarry showing large-scale trough cross-stratification. B) Detail of large-scale trough -stratification in TCS facies. Outcrop above stratigraphic column A.

Burrowed and Massive Sandstone (BMS). This facies encompasses trough cross-stratified sandstones of varying preservation quality and degrees of bioturbation including massive sandstones, burrowed sandstones, and trough cross-stratified sandstones where nothing finer than decimeter-scale laminations have been preserved. Depending on location, this facies can be very pale orange, similar to interdune sediments, or bluish white like the TCS facies. Weathered exposures are commonly pockmarked, where pockmarks can be up to 13 cm across (Fig. 12CB). Invertebrate burrows, when discernable are straight, non-branching, and vertical, but sometimes horizontal (Fig. 12C and D). The burrows are 5 to 8 mm in diameter. Burrow fill is darker than the surrounding sediment. Good and Ekdale (2014) provide a detailed study of these burrows at Saints & Sinners Quarry. A new previously undescribed burrow (Fig. 12A) is 15 cm long and nearly 10 cm in diameter. This large burrow is unrelated to the smaller burrows and is present in only one location. Sporadic millimeter to centimeter cm thick iron lamina and circular iron concretions are common in massive beds. This facies outcrops immediately above and below interdune sediments, and is up to 7 m thick.
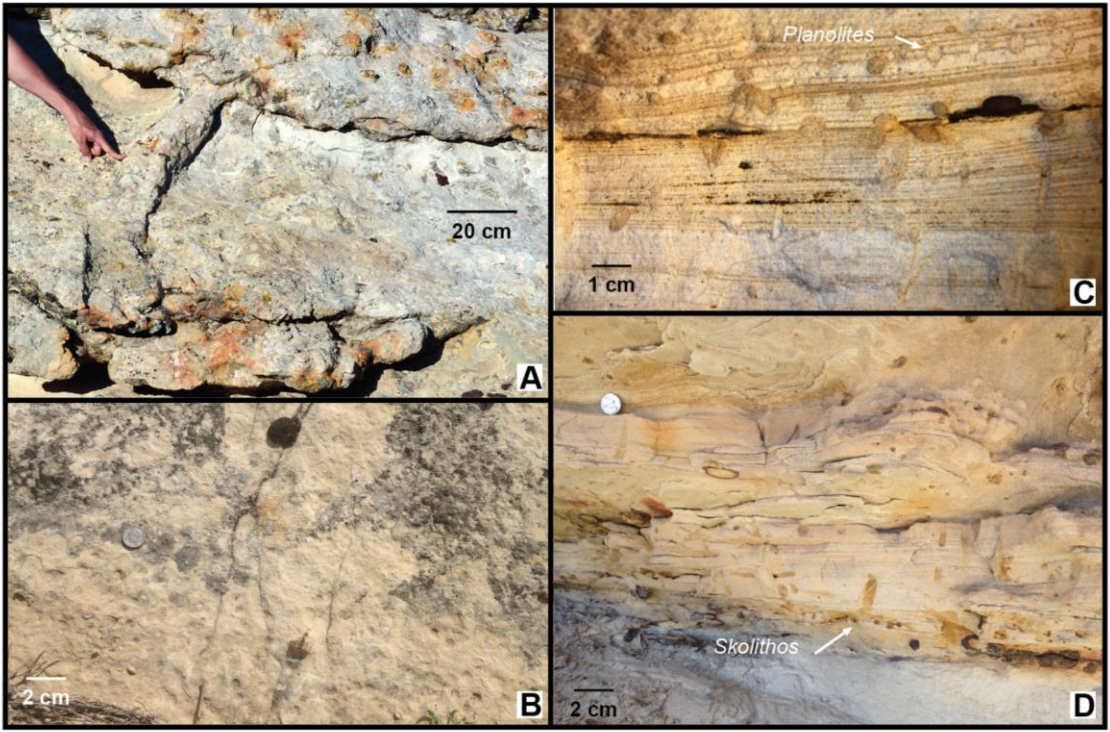
Figure 12 Burrowed and Massive Sandstone facies. A) Previously undescribed large burrow attributed to an unknown vertebrate maker. The pockmarked surfaces are typical of moderately bioturbated dunes. B) Pockmarked weathering texture typical of near horizontal exposures of bioturbated horizons. C) Burrows in trough cross-stratified sandstone below the interdune sediments. D) Burrows in trough cross-stratified sandstone above interdune sediments

FACIES DISTRIBUTION

A succinct explanation of the facies distribution and relationships will aid in their depositional interpretation discussed later. Through observing the distribution and relationship of interdune facies in the photogrammetric model and walking along the outcrop, it is apparent that the interdune facies at Saints & Sinners Quarry are preserved in a wedge-shaped package (Fig 13). This interdune wedge is thickest at stratigraphic column A (Fig. 5) and thins northward and eastward. The wedge measures 320 m north to south and 50 m east to west. The wedge is truncated to the north and south by ravines developed along faults or joints. To the west the wedge dips into the subsurface, while the eastern boundary is lost to erosion. The wedge is bounded above and below by Trough Cross-Stratified Sandstone (TCS) or Burrowed and

23

Massive Sandstone (BMS) dune facies (Fig. 13A). The strata below the wedge are mostly TCS facies; except for the area west of stratigraphic column B (Fig. 5) where the TCS facies transitions into the BMS facies. At southern stratigraphic columns, A, B and C (Figure 5) the BMS facies overlies the interdune with a decrease in bioturbation moving eastward and northward. North of the quarry, the BMS facies transitions into the TCS facies so that at stratigraphic column D, the TCS facies overlies the interdunal wedge.

The base of the interdunal wedge is marked by a planar surface on which the Wavy Sandstone Facies (WSS) facies is preserved. The WSS facies is thickest at stratigraphic column A in Figure 5 and thins to the east (stratigraphic columns B and C) and north (stratigraphic column D). It is the only interdune facies present at stratigraphic column D (Fig. 5) where it has thinned to 15 cm from 160 cm at stratigraphic column A. This facies is traceable over the geographic extent of the outcrop and is the most widespread interdune facies covering at least 12,700 m^2. On top of this is the Green Claystone and Siltstone (GCS) facies. Again, this facies is generally thicker at stratigraphic column A (Fig 5) and thins to the north, east, and west. Occurrences of this facies pinch out at the quarry and are not present at stratigraphic column C or D. Between beds of the GCS facies are beds of the Planar Laminated Sandstone (PLS) and Massive Bone Bed Facies (MBB) facies. The PLS facies is again thicker at stratigraphic column A and thins to the north and east. A few meters before start column B, the PLS facies transitions into the MBB. The facies pinches out at the quarry and is not present at stratigraphic column C or D. At some locations, the WSS facie overlies GCS and MBB or PLS facies couplets.
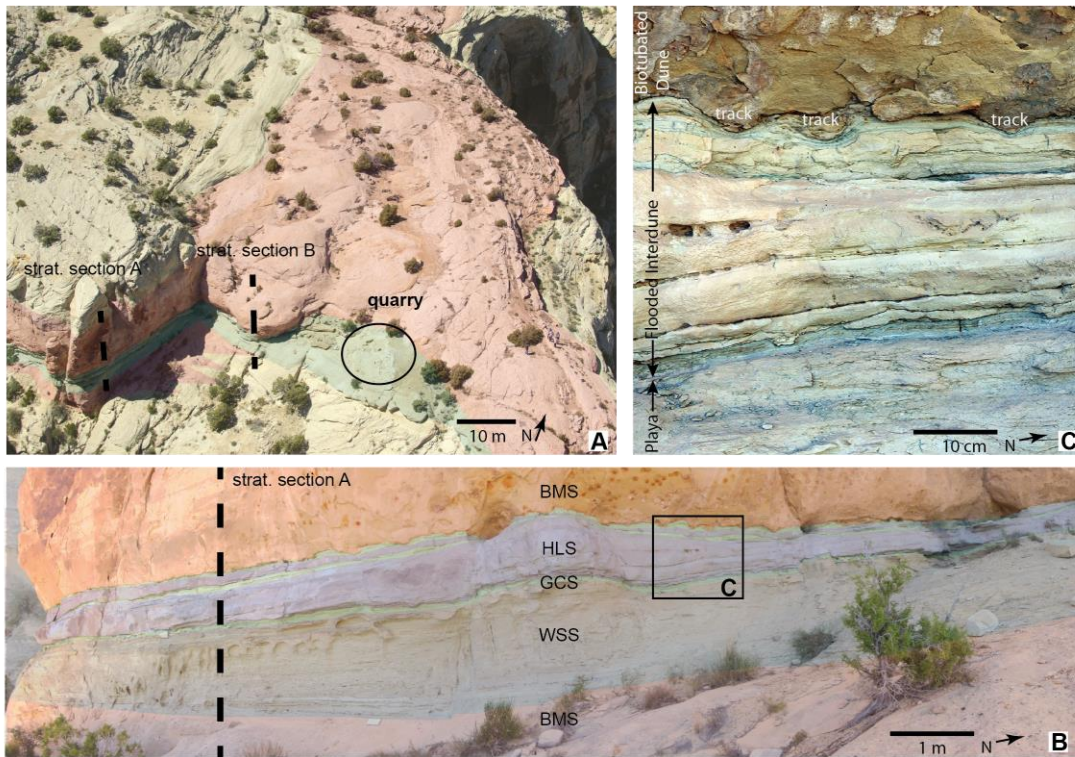
Figure 13 Facies distribution. A) Facies mapped on Figure 2B with stratigraphic section locations indicated by dashed white lines. Interdune facies are in green, TCS facies are in yellow and BMS facies in pink. Interdune facies are present to the north of the quarry below the upper BMS facies but are not visible at this angle. The interdune sediments are preserved in wedge shape that thins to the north and east. B) Interdune facies distribution near stratigraphic column A (shown in dashed line). C) Detail of flooded interdune facies.

BONE DISTRIBUTION

Bones have been identified and excavated in a roughly 19 m^2 area of the quarry. Bones are

preserved in three distinct superposed units of Massive Bone Bed Facies (MBB) facies

essentially devoid of sedimentary structures (Fig. 10A). Units are separated by sub-mm-thick

clay/silt parting planes of the GCS facies. These parting planes aid in the extraction of slabs of

the MBB. Quarry bones are not evenly distributed vertically or laterally. Bones of smaller taxa

are found from the top of bone bed 1 to the middle of bone bed 2. While bones of larger taxa are

common in the middle of bone bed 2, they are more abundant in bone bed 3. The orientation of

bones and skeletons ranges from random in bone beds 1 and 2 to substantially oriented in bone

bed 3 (Britt et al., 2011; Chambers et al., 2011). Bone beds can therefore predict to a certain degree bone orientation and taxa size.

FACIES INTERPRETATION

Interdune Facies Interpretation

Wavy and Wrinkly Sandstone (WSS). This facies is interpreted as a dry and damp playa pan. The wavy and wrinkle laminations that characterize this facies are interpreted as a combination of adhesion (Kocurek and Fielder, 1982) and microbial or algal structures (Eisenberg, 2003; Hagadorn and Bottjer, 1999). Trough cross-stratified sets are interpreted as avalanche deposits of small eolian dunes (Ahlbrandt and Fryberger, 1981). A water table near the surface of the playa pan provided favorable conditions for algal growth and adhesion structures (Fryberger et al., 1983). However, small eolian dunes, common in drier conditions, indicate the playa experienced a fluctuating water table.

Green Claystone and Siltstone (CSC). The green claystone and siltstone are interpreted as deposits from quiet standing water in a flooded interdune (Ryang and Chough, 1997). A lack of desiccation features suggests water was continually present, and that this facies was likely deposited in an interdune oasis or lake (Gradziński and Jerzykiewicz, 1974). Sediment loading (Crabaugh and Kocurek, 1993) (Ahlbrandt and Fryberger, 1981), and bioturbation such as footprints, or some combination of the two are likely causes of undulations and undulatory contacts.

As previously stated, RockJock11 results indicate an average of 31% clay in the green claystone and siltstone facies. The average degree of fit between the RockJock 11 calculated curves and the measured XRD curves was 0.1802. Normalized results indicate 28.9% clays by average weight

percent. Clays by average weight percent include illite (1M; R>3; 95%I) 15.6%, muscovite 6.1%, and illite (R>1; 70-80%I) 7.2%. On average, normalized results indicate non-clay minerals account for 71.1%, and include by average weight percent quartz 53.6%, intermedieate microcline kspar 13%, dolmite 2.8%, and calcite 1.8% (See Appendix A).

Unmatched or poorly matched peaks explain the relatively poor degree of fit between the calculated and measured XRD curves. Peaks at or near 8.9, 12.5, 23.5, 25.4, 32.2, and 48.0 two theta were not matched or poorly matched by RockJock11. RockJock 11 includes a table from Brown and Brindley (1980) to correlate peaks and minerals. Unmatched peaks correlated to the following minerals; collapsed smectite at 8.9 two theta, green rust at 23.5 two theta, glycerol smectite at 25.4, and gamma alumina at 32.2 and 48.0 two theta. These peaks were left unmatched because RockJock11 is not capable of solving for these minerals. The unmatched smectite peaks indicate there are possibly more clays than the calculated 28.9%. The aluminum insert used to decrease the volume of the sample holder likely caused gamma alumina peaks. The green rust peak fits well considering the green outcrop color. The peak at 12.5 two theta is poorly matched in some samples and unmatched in others. In samples where the peak is poorly matched, it correlates to a small illite peak. Using the table from Brown and Brindley (1980) included with RockJock11, this peak also correlates to a number of other minerals including dickite and serpentine. However, when selected as inputs, these minerals are not present in the measured XRD profile. The 12.5 two theta peak is therefore likely just a poorly matched illite peak.

Planar Laminated Sandstone (PLS). The planar laminated sandstone is bounded above and below by the green claystone and siltstone facies and is interpreted as flooded interdune suspension fall out during haboob and other windstorms. Haboob, Arabic for "strong wind", describes a weather phenomenon characterized by immense walls of blowing sand and dust. They are common in present day mid-latitude desserts during spring and summer when monsoonal moisture combines with increased insolation (Miller et al., 2008). These storm were likely common in ancient mid-latitude deserts with monsoonal characteristics such as the Nugget Sandstone (Loope et al., 2001). Particles originating from a distant source and transported via haboob have a median grain size of 5 µm (very fine silt) to 35 µm (coarse silt) (Gillies et al., 1996; Chen and Fryrear, 2002). Early stage haboobs have a distribution of tens to hundreds of µm (fine silt to coarse sand) (Miller et al., 2008). Sand grains, very fine to fine sand, in this facies would have been transported in the early stage of haboob. The sands of the PLS facies were likely not transported far, but blown in from adjacent dunes into the flooded interdune during haboobs and other strong wind events.

Massive Bone Bed Sandstone (MBB). A thinning GCS facies, relict ripple-like structures, and preferential bone orientation indicate this facies was deposited near the shoreline of an ancient lake. Sands were deposited during haboob storms and other wind events that also deposited the planar laminated sandstone facies. Shoreline processes subsequently reworked the sands causing ripple like structures and preferentially orientated bones. During times of quiescence, silts and clays settled out of the water and accumulated as the GCS facies. Moderate bioturbation likely destroyed most primary sedimentary structures.

Trough Cross-Stratified Sandstones (TCS). The large and small scale trough cross-stratified sandstones of the Nugget Sandstone have long been interpreted as deposits of migrating dunes (Picard, 1975). Observations from this study agree with previous interpretations.

Burrowed and Massive Sandstone (BMS). Where preserved, primary sedimentary structures including large-scale trough cross-stratification indicate eolian dune deposition. Bioturbation altered primary structures where decimeter-scale laminas are the only lamina preserved. Massive units are interpreted to be highly bioturbated. Burrows present in moderately bioturbated strata have previously been interpreted as *Skolithos* and *Planolites* (Good and Ekdale, 2014). The pockmarked weathering is attributed to the lack of sedimentary structures and could possibly be related to larger burrows, such as the large vertebrate burrow (Fig 9A). Sporadic hematite laminas in massive beds are interpreted as deflation surfaces, now accentuated by post-depositional hematite. Deflation surfaces, relict cross-stratified beds, and undisturbed contact with underlying units indicate bioturbation as a more likely cause of massive sands than liquefaction.
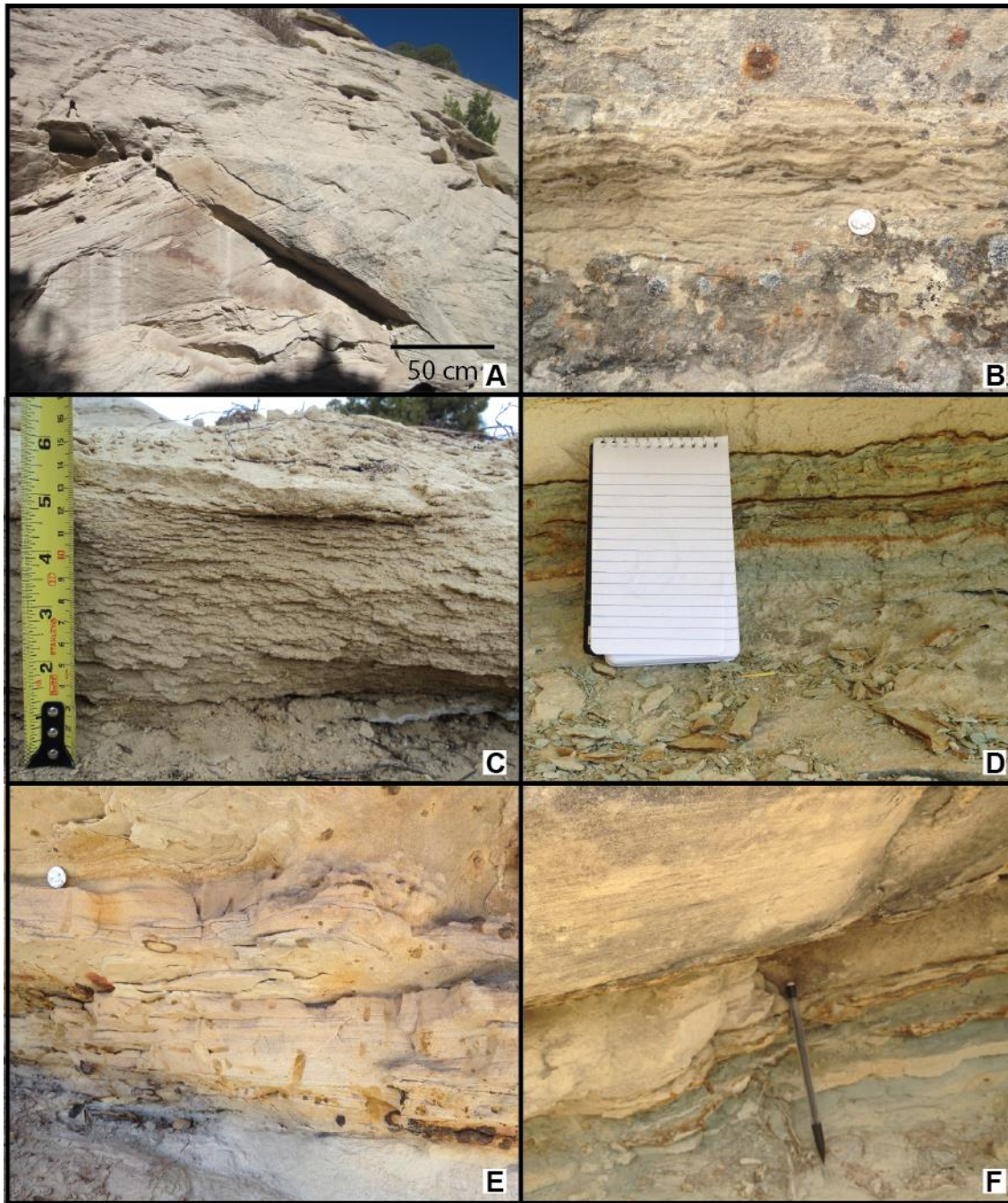
Figure 14 Facies overview. A) TCS facies. B) WSS facies. C) MBB facies. D) GCS facies. E) BMS facies. F) PLS facies

DISCUSSION

Depositional History

The depositional history of the Saints & Sinners interdune complex can be interpreted from the facies (Fig. 14, Table 2) and their spatial relationships (Figs. 13 and 15). Interdune sediments are deposited in a wedge-shape that thins to the north and east. Sediments below this wedge suggest dry eolian deposition dominated by large dune deposits existed before the development of the interdune.

Eolian deposition is strongly dependent on changes of the water table height. Changes of the water table can occur due to changes in climate, subsidence rates, sedimentation rates, or any combination of the three (Fryberger, 1990; Kocurek and Havholm, 1993). Deflation of dune sediments down to the capillary fringe likely created the expansive flat area/playa pan on which the interdune facies later accumulated. Following the development of the pan organisms burrowed into underlying dunes resulting in the Bioturbated and Massive Sandstone (BMS) facies below the interdune wedge. The Wavy Sandstone (WSS) facies is the first and most widespread (a minimum of 12,700 sq. m) interdune facies. During deposition of the WSS facies the water table and capillary fringe fluctuated near the interdune surface. When the water table or capillary fringe was below the surface small eolian dunes migrated across and accumulated on the flats. A water table or capillary fringe near the surface provided favorable conditions for algal growth and adhesion structures (Fryberger et al., 1983).
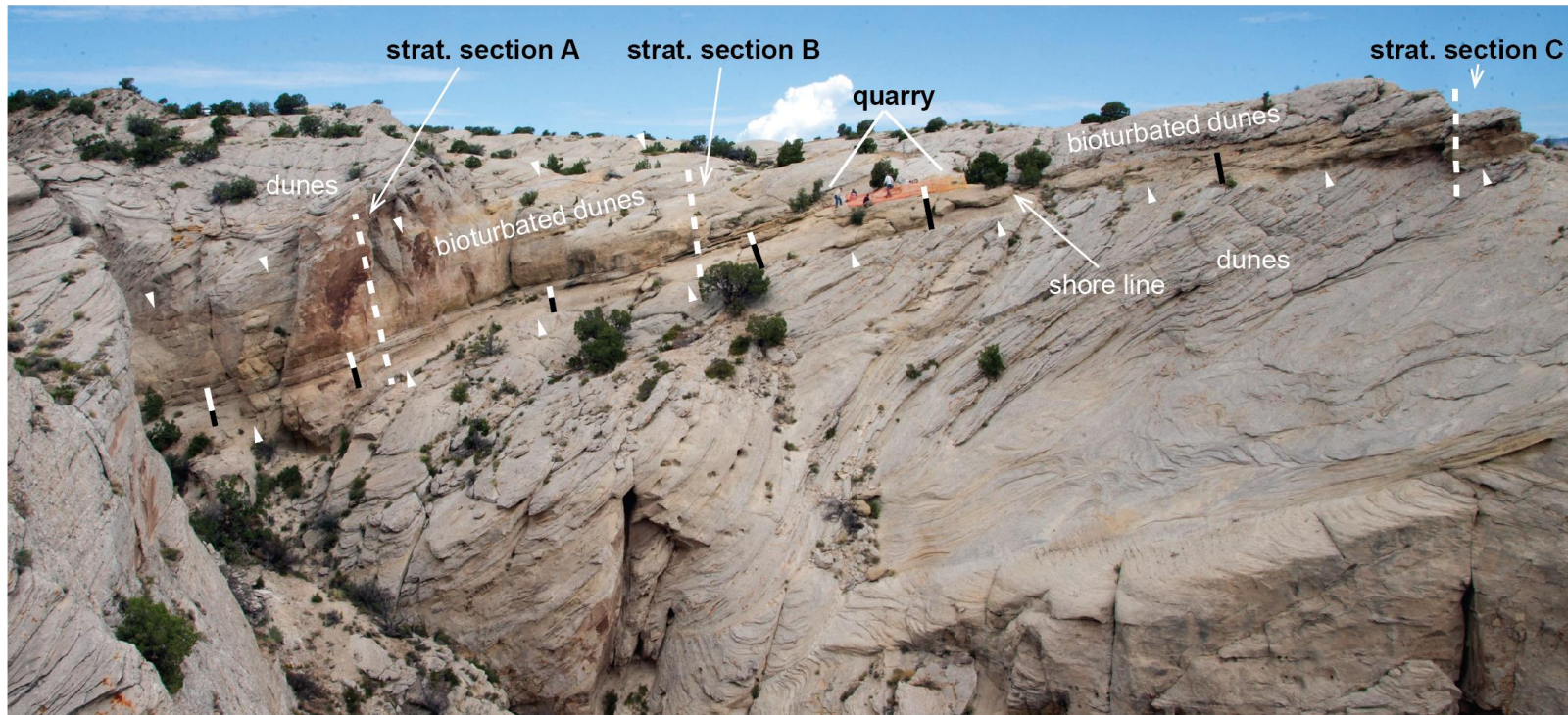
Figure 15 Depositional overview. View of quarry area looking north northwest annotated with depositional environments. Stratigraphic columns (dashed lines) are detailed in Figure 5. White triangles bound the bioturbated dune strata. Bars indicate interdune sediments, white bars highlight lacustrine interdune sediments; black bars highlight damp interdune/playa sediments. A shoreline is interpreted at the point where lacustrine interdune sediments pinch out. The quarry is in shallow waters near the shoreline. Figure modified from (Britt et al., 2016). Photo by Mark Philbrick.

A continual relative rise in the water table allowed for the deposition and preservation of the WSS facies (Kocurek and Havholm, 1993). Eventually, the water table increase outpaced the sediment supply, and the southern portion of the interdune flooded depositing the first occurrence of the Green Claystone and Siltstone (GCS) facies. A continual rise in the water table, without an increase of sediment supply, is known to lead to shaley lacustrine sedimentation in interdunes (Fryberger, 1990). These facies are thickest to the southwest of the quarry near stratigraphic column A in Figure 5 suggesting more accommodation and deeper water. The GCS thins to the north, indicating shallower water and less accommodation. The shoreline is interpreted to occur just to the east of the quarry where the GCS bed laminae terminate. These beds were deposited during times of quiet water with minimal sand input.

The Planar Laminated Sandstone (PLS) facies and Massive Bone Bed (MBB) facies were also deposited in the flooded interdune. During times of quiet water the GCS facies was deposited; but, during haboobs and other windstorms, the interdune lake trapped wind blown sediment that came in contact with the water's surface. The trapped wind blown sediment was deposited as the PLS facies in the lake (stratigraphic column A and B) and the laminae are here interpreted as trapped pulses of sediment related to major gusts of wind in deeper water below wave depth. The MBB facies accumulated in a similar matter, but in shallower water near the shoreline where wave action impacted the lake bottom, hence the preservation of ripples at the bottom of bone bed 1, and relics of ripples at the bottom of bone beds 2 (Fig. 9) and 3. Bioturbation along the shore likely destroyed most of the sedimentary structures in these beds. The bone beds were deposited during three storm events. Details of their interpreted depositional environment are in the next section.

Over time, the relative water table fell. With this, the water receded and the interdune returned to the playa pan environments of the WSS facies. Tridactyl foot prints (Fig. 6C and Fig. 5 stratigraphic column B) are preserved in the wrinkle laminations from this time. As the relative water table continued to fall, dunes began to migrate over the lake. Organisms bioturbated, to varying degrees, the dunes overlying the southern interdune wedge. Dunes were moderately bioturbated to the east of the lake at stratigraphic column C (Fig. 5), allowing the preservation of burrows. Heavy bioturbation towards the center of the now gone lake near stratigraphic columns A and B (Fig. 5) left only massive sands with deflation surfaces accentuated by post dispositional hematite. Both the moderately bioturbated and massive sediments are part of the BMS facies. In the end, the environment returned to its original state - a dry eolian system dominated by large dune deposits of the TCS facies.

Bone Bed Depositional History

A detailed study of the bones, taxonomy, and taphonomy is not undertaken here — the purpose of this thesis is to provide a geologic foundation for a future, detailed taphonomic analysis of the bone beds. The three superimposed MBB facies units that contain bones are interpreted to have been deposited by sand blown into shallow, standing water during haboobs or local windstorms. The green clays on top of each of the bone beds mark a time of quiescence that allowed the fine silts and clays to settle. The quarry is interpreted to be along the shore of the lake because lake associated faces pinch just east of the bone beds but thicken to the west. The large number of animals and the taxonomic diversity of the fauna suggest a mass die off, likely caused by drought (). The first sand blown into the rising lake waters buried small carcasses intact. Larger carcasses were not immediately buried but macerated in the shallows, where wave action reworked

34

oriented and disarticulated the bones until they were buried by later sand storms. The increase in orientation of bones in the uppermost bone bed suggests reworking by wave action.

CONCLUSIONS

The Saints & Sinners Quarry in northeastern Utah is a unique paleontology site. It has yielded over 18,000 bones, including the only known body fossils from the Nugget Sandstone. It also preserves the most diverse fauna known from the Late Triassic to Middle Jurassic North American erg systems. (Chure et al., 2014; Rowland and Mercadante, 2014; Good and Ekdale, 2014; Wilkens et al., 2007; Irmis, 2005; Tykoski, 2005; Sues et al., 1994). Additionally, the presence of drepanosaurs and procolophonids provide the most convincing evidence to-date that the lower portions of the formation are Late Triassic in age. The geologic facies analysis presented in this work divides the quarry's strata into six facies. The various facies and their spatial relationships are interpreted as an interdune that at times was partly occupied by a lake. The interdune flat likely developed by deflation down to or near the capillary fringe. The relative water table then rose and part of the interdune flat was flooded to create an interdune lake. The fossil assemblage suggests a single drought sourced the bones now preserved in the quarry. The bones were buried along the shore of the lake, some being oriented by wave action. Ultimately, the interdune was buried by continued or renewed migration of the dunes.

This thesis has laid the geologic foundation necessary for future taphonomy and paleontology work that will provide further insights into the preservation of the bones. Determining the age of the bones through paleontology has broad implications for better controlling the age of the Nugget Sandstone and delineating the position of the Triassic-Jurassic boundary in northeastern Utah and adjacent states.

REFERENCES

Ahlbrandt, T.S., and Fryberger, S.G., 1981, Sedimentary features and significance of interdune deposits: SEPM Special Publication, p. 293–314.

Blakey, R.C., and Gubitosa, R., 1983, Late Triassic paleogeography and depositional history of the Chinle Formation, southern Utah and northern Arizona: Rocky Mountain Paleogeography Symposium, p. 57–76.

Blender. 2.76. Blender Foundation.

Britt, B., Chambers, M., Engelmann, G., Chure, D., and Scheetz, R., 2011, Taphonomy of Coelophysoid theropod bonebeds preserved along the shoreline of an Early Jurassic lake in the Nugget Sandstone of NE Utah, *in* Journal Of Vertebrate Paleontology, Society of Vertebrate Paleontology, p. 78.

Britt, B.B., Chure, D.J., Engelmann, G.F., and Shumway, J.D.S., 2016, Rise of the erg— paleontology and paleoenvironments of the Triassic – Jurassic transition in northeastern Utah: Geology of the Intermountain West, v. 3.

Brown, G. T, and Brindley, G.W., 1980, X-ray diffraction procedures for clay mineral identification: Crystal structures of clay minerals and their X-ray identification, v. 5, p. 305–359.

Chambers, M., Kimberly, H., Britt, B.B., Chure, D.J., Engelmann, G.F., and Scheetz, R., 2011, Preliminary taphonomic analysis of a Ceolophysoid theropod dinosaur bonebed in the Early Jurassic Nugget Sandstone of Utah, *in* Geological Society of America Abstracts with Programs, p. 16.

Chen, W., and Fryrear, D.W., 2002, Sedimentary characteristics of a haboob dust storm: Atmospheric Research, v. 61, p. 75–85, doi: 10.1016/S0169-8095(01)00092-8.

Chure, D.J., Good, T.R., and Engelmann, G.F., 2014, A forgotten collection of vertebrate and invertebrate ichnofossils from the Nugget Sandstone (Late Triassic-Early Jurassic), near Heber, Wasatch County, Utah: New Mexico Museum of Natural History and Sciesces Bulletin, v. 62, p. 181–196.

Cisneros, J.C., 2008, Phylogenetic relationships of procolophonid parareptiles with remarks on their geological record: Journal of Systematic Palaeontology, v. 6, p. 345–366.

Committee., R.-C.C., and America., G.S. of, 1991, Rock-color chart: Boulder, Colo., Distributed by Geological Society of America.

Crabaugh, M., and Kocurek, G., 1993, Entrada Sandstone: an example of a wet aeolian system: Geological Society, London, Special Publications, v. 72, p. 103–126, doi: 10.1144/GSL.SP.1993.072.01.11.

Dickinson, W.R., 2004, Evolution of the North American cordillera: Annual Review of Earth and Planetary Science., v. 32, p. 13–45.

Dickinson, W.R., and Gehrels, G.E., 2009, U-Pb ages of detrital zircons in Jurassic eolian and associated sandstones of the Colorado Plateau: Evidence for transcontinental dispersal and intraregional recycling of sediment: Geological Society of America Bulletin, v. 121, p. 408–433.

Doelger, N.M., 1987, The stratigraphy of the Nugget Sandstone, *in* The Thrust Belt Revisited; 38th Annual Field Conference Guidebook,.

Dubiel, R.F., 1994, Triassic deposystems, paleogeography, and paleoclimate of the Western Interior: Mesozoic systems of the Rocky Mountain region, USA, p. 133–168.

Eberl, D.D., 2003, User guide to RockJock-A program for determining quantitative mineralogy from X-ray diffraction data: US Geological Survey RPRT.

Eisenberg, L., 2003, Giant stromatolites and a supersurface in the Navajo Sandstone, Capitol Reef National Park, Utah: Geology, v. 31, p. 111–114, doi: 10.1130/0091-7613(2003)031<0111:GSAASI>2.0.CO;2.

Fryberger, S.G., 1990, Role of water in eolian deposition: modern and ancient eolian deposits: Petroleum Exploration and Production, p. 7–15.

Fryberger, S.G., Al-sari, A.M., and Clisham, T.J., 1983, Eolian dune, interdune, sand sheet, and silicilastic sabkha sediments of an offshore prograding sand sea, Dharan Area, Saudi Arabia: American Association of Petroleum Geologists Bulletin, v. 67, p. 280–312.

Gillies, J.A., Nickling, W.G., and McTainsh, G.H., 1996, Dust concentrations and particle-size characteristics of an intense dust haze event: inland delta region, Mali, West Africa: Atmospheric Environment, v. 30, p. 1081–1090.

Good, T.R., 2013, Life in an ancient sea of sand: trace fossil associations and their paleoecological implications in the Uppper Triassic/Lower Jurassic Nugget Sandstone, northeaster Utah [Masters thesis]: The Univeristy of Utah.

Good, T.R., and Ekdale, A.A., 2014, Paleoecology and taphonomy of trace fossils in the eolian Upper Triassic / Lower Jurassic Nugget Sandstone , northeastern Utah: Palaios, v. 29, p. 401–413.

Gradziński, R., and Jerzykiewicz, T., 1974, Dinosaur- and mammal-bearing aeolian and associated deposits of the Upper Cretaceous in the Gobi Desert (Mongolia): Sedimentary Geology, v. 12, p. 249–278, doi: 10.1016/0037-0738(74)90021-9.

Gregory, H.E., and Moore, R.C., 1931, The Kaiparowits region, a geographic and geologic reconnaissance of parts of Utah and Arizona: U.S. Geological Survey Professional Paper 164, 161 p., 3 plates.

Hagadorn, J.W., and Bottjer, D.J., 1999, Restriction of a Late Neoproterozoic biotope: suspect-
microbial structures and trace fossils at the Vendian-Cambrian transition: Palaios, v. 14, p.
73, doi: 10.2307/3515362.

High Jr, L.R., and Picard, M.D., 1975, Sedimentary cycles in the Nugget Sandstone, northeastern
Utah: Utah Geology, v. 2:

Irmis, R.B., 2005, A review of the vertebrate fauna of the Lower Jurassic Navajo Sandstone in
Arizona: Vertebrate Paleontology of Arizona: Mesa Southwest Museum Bulletin, v. 11, p.
55–71.

Irmis, R.B., Chure, D.J., Engelmann, G.F., and Wiersma, J.P., 2015, The alluvial to eolian
transition of the Chinle an Nugget Formations in the southern Uinta Mountains,
northeastern Utah., *in* Vanden Berg, M.D., Ressetar, R., and Birgenheier, L.P. eds., Geology
of Utah's Unita Basin and Uinta Mountains, Utah Geological Association Publication, p.
13–48.

Irmis, R.B., Mundil, R., Martz, J.W., and Parker, W.G., 2011, High-resolution U-Pb ages from
the Upper Triassic Chinle Formation (New Mexico, USA) support a diachronous rise of
dinosaurs: Earth and Planetary Science Letters, v. 309, p. 258–267, doi:
10.1016/j.epsl.2011.07.015.

Kent, D. V, and Irving, E., 2010, Influence of inclination error in sedimentary rocks on the
Triassic and Jurassic apparent pole wander path for North America and implications for
Cordilleran tectonics: Journal of Geophysical Research: Solid Earth, v. 115.

Kent, D. V, and Tauxe, L., 2005, Corrected Late Triassic latitudes for continents adjacent to the
North Atlantic: Science, v. 307, p. 240–244.

Kinney, D.M., 1955, Geology of the Uinta River-Brush Creek area, Duchesne and Uintah

Counties, Utah: U.S. Geological Survey Bulletin 1007, 185 p., scale 1:63,360

Knapp, R.R., 1978, Depositional environments and diagenesis of the Nugget Sandstone : south-central Wyoming , northeast Utah and northwest Colorado, *in* Resources of the Wind River Basin; 30th Annual Field Confernce Guidebook, p. 131–138.

Kocurek, G., and Dott Jr., R.H., 1983, Jurassic paleogeographic and paleoclimate of the central and southern Rocky Mountains region: Mesozoic Paleogeography of West-Central United States, p. 101–116.

Kocurek, G., and Fielder, G., 1982, Adhesion structures: Sedimentary Petrology, v. 52.

Kocurek, G., and Havholm, K.G., 1993, Eolian sequnce stratigraphy - a conceptual framework, *in* Recent Advances in and Applications of Siliciclastic Sequence Stratigraphy, American Association of Petroleum Geologists Memoir, p. 393–409.

Kowallis, B.J., Christiansen, E.H., Deino, A.L., Zhang, C., and Everett, B.H., 2001, The record of Middle Jurassic volcanism in the Carmel and Temple Cap Formations of southwestern Utah: Geological Society of America Bulletin, v. 113, p. 373–387.

Lockley, M.G., Conrad, K., and Paquette, M., 1992, New discoveries of fossil footprints at Dinosaur National Monument: Park Science, v. 12, p. 4–5.

Loope, D.B., and Rowe, C.M., 2003, Long-lived pluvial episodes during deposition of the Navajo Sandstone: The Journal of Geology, v. 111, p. 223–232, doi: 10.1086/345843.

Loope, D.B., Rowe, C., and Joeckel, R., 2001, Annual monsoon rains recorded by Jurassic dunes: Nature, v. 412, p. 5–7.

Lucas, S.G., and Heckert, A.B., 2011, Late Triassic aetosaurs as the trackmaker of the tetrapod footprint ichnotaxon Brachychirotherium: Ichnos, v. 18, p. 197–208.

Marzolf, J.E., 1988, Controls on late Paleozoic and early Mesozoic eolian deposition of the

western United States: Sedimentary Geology, v. 56, p. 167–191, doi: 10.1016/0037-0738(88)90053-X.

May, S.B., 2014, The Bell Springs Formation: characterization and correlation of Upper Triassic Strata in Northeast Utah:

Miller, S.D., Kuciauskas, A.P., Liu, M., Ji, Q., Reid, J.S., Breed, D.W., Walker, A.L., and Mandoos, A. Al, 2008, Haboob dust storms of the southern Arabian Peninsula: Journal of Geophysical Research Atmospheres, v. 113, p. 1–26, doi: 10.1029/2007JD008550.

Milligan, M., 2012, Sizing up titans - Navajo erg vs. Sahara ergs. Which was the larger sand box? Title: Utah Geological Survery, Survey Notes, v. 44, p. 8–9.

Momento. Beta Version. Autodesk.

Omotoso, O., and Eberl, D., 2009, Sample preparation and data collection strategies for X-ray diffraction quantitative phase analysis of clay-bearing rocks, *in* 46th Annual Meeting of The Clay Minerals Society,.

Picard, M.D., 1975, Facies, petrography and petroleum potential of Nugget Sandstone (Jurassic), southwestern Wyoming and northeastern Utah, *in* Symposium on deep drilling frontiers of the central Rocky Mountains: Rocky Mountain Association of Geologists Guidebook, p. 109–127

Poole, F.G., and Stewart, J.H., 1964a, Chinle Formation and Glen Canyon Sandstone in northeastern Utah and northwestern Colorado, in Sabatka, E.F., editor, Guidebook to the geology and mineral resources of the Uinta Basin, Utah's hydrocarbon storehouse: Intermountain Association of Petroleum Geologist 13th Annual Field Conference, p. 93-104.

Poole, F.G., and Stewart, J.H., 1964, Chinle Formation and Glen Canyon Sandstone in
northeastern Utah and northwestern Colorado: U.S. Geological Survey Professional Paper
501-D, p. D30-D39.

Powell, J.W., 1876, Report on the geology of the eastern portion of the Uinta Mountains and a
region of country adjacent thereto: U.S. Geological and Geographical Survey of the
Territories (Powell), 218 p.

ReCap. 2016. Autodesk.

Renesto, S.C., Spielmann, J.A., and Lucas, S.G., 2009, The oldest record of drepanosaurids
(Reptilia, Diapsida) from the Late Triassic (Adamanian Placerias Quarry, Arizona, USA)
and the stratigraphic range of the Drepanosauridae: Neues Jahrbuch für Geologie und
Paläontologie-Abhandlungen, v. 252, p. 315–325.

Riggs, N.R., Lehman, T.M., Gehrels, G.E., and Dickinson, W.R., 1996, Detrital zircon link
between headwaters and terminus of the Upper Triassic Chinle-Dockum paleoriver system:
Science, v. 273, p. 97.

Rowland, S., and Mercadante, J., 2014, Trackways of a gregarious, dunefield-dwelling, Early
Jurassic therapsid in the Aztec Sandstone of southern Nevada: Palaios, p. 539–552.

Ryang, R.H., and Chough, S.K., 1997, Sequential development of alluvial/lacustrine system:
southeastern Eumsung Basin (Cretaceous), Korea: Journal of Sedimentary Research, v. 67,
p. 274–285.

Sprinkel, D. A., Kowallis, B. J., & Jensen, P. H. 2011. Correlation and age of the Nugget
Sandstone and Glen Canyon Group, Utah, in Sprinkel, D.A., Yonkee, W.A., and Chidsey,
T.C., Jr., editors, Sevier thrust belt: northern and central Utah and adjacent areas. Utah
Geological Association Publication 40, p. 131-149

Srodon, J., Drits, V.A., McCarty, D.K., Hsieh, J.C.C., and Eberl, D.D., 2001, Quantitative X-ray diffraction analysis of clay-bearing rocks from random preparations: Clays and Clay Minerals, v. 49, p. 514–528.

Stewart, J.H., Poole, F.G., Wilson, R.F., Cadigan, R.A., Thordarson, W., and Albee, H.F., 1972, Stratigraphy and origin of the Chinle Formation and related Upper Triassic strata in the Colorado Plateau region: Geological Survey (US) RPRT.

Sues, H.-D., Clark, J.M., Jenkins Jr, F.A., Fraser, N.C., and Sues, H.D., 1994, A review of the Early Jurassic tetrapods from the Glen Canyon Group of the American Southwest: In the shadow of the dinosaurs: Early Mesozoic tetrapods, v. 283.

Tykoski, R.S., 2005, Vertebrate paleontology in the Arizona Jurassic: Mesa Southwest Museum Bulletin, v. 11, p. 72–93.

Veatch, A. C. 1907. Geographyand Geology of a portion of southwestern Wyoming. U.S. Geological Survey Professional Paper 56, 178 p.

Wilkens, N.D., Farmer, J.D., and Pigg, K.B., 2007, Paleoecology of Early Jurassic Navajo Sandstone interdune deposits: Geological Society of America, p. 417.
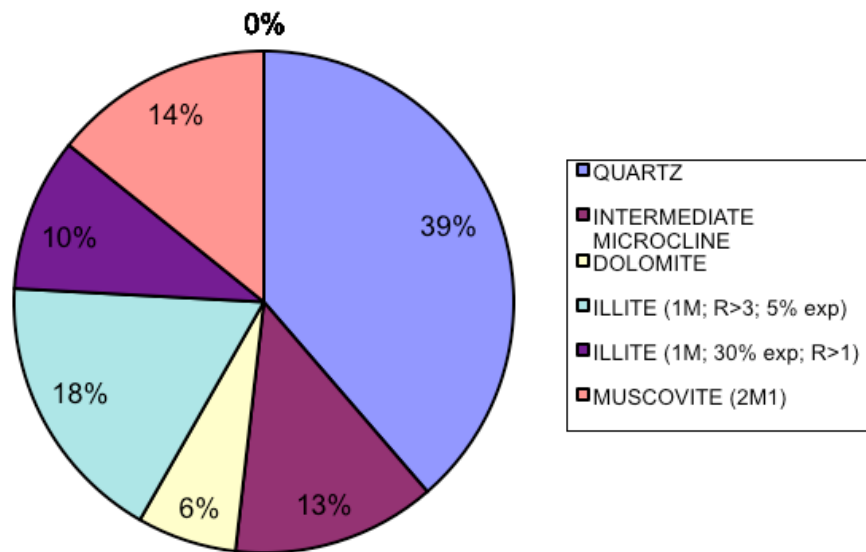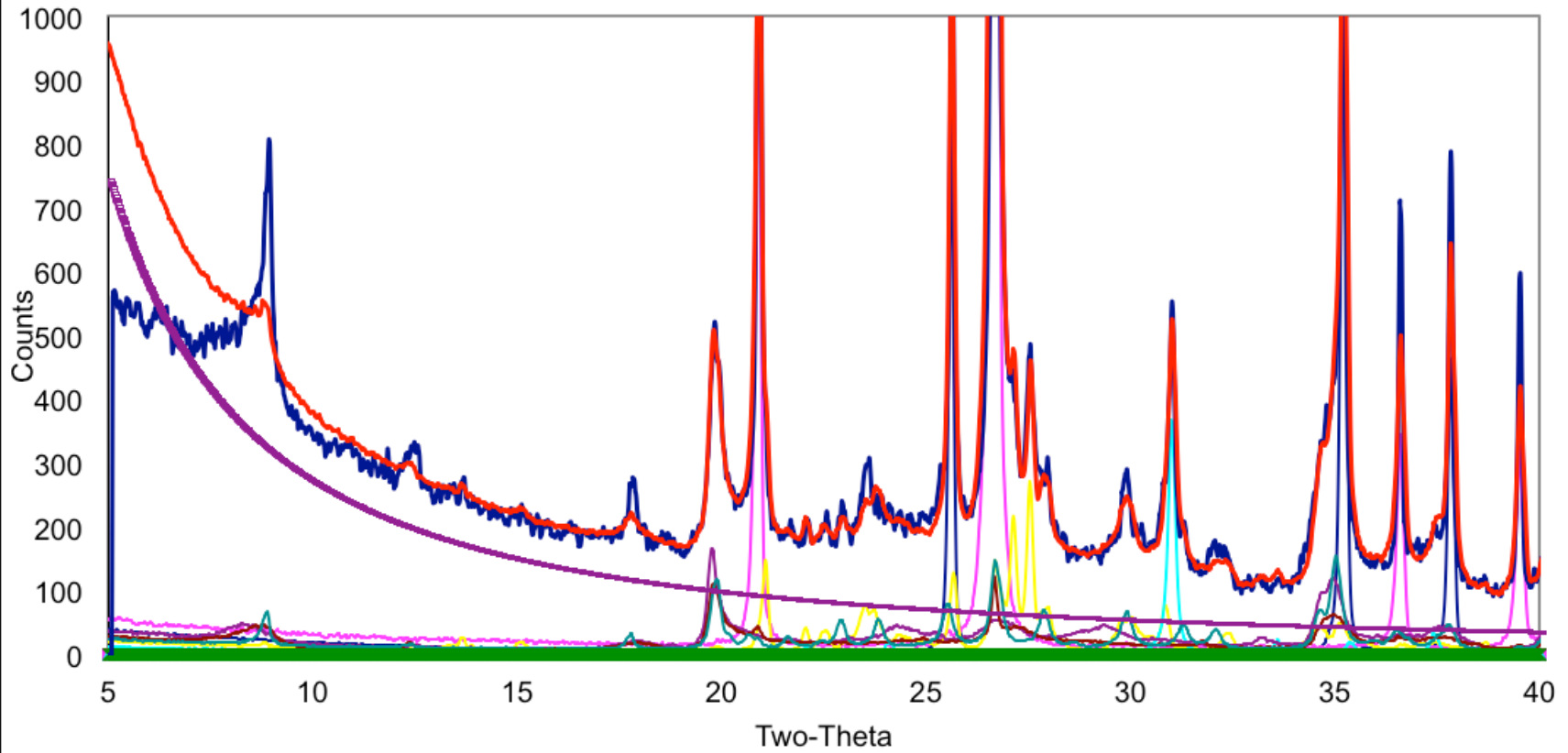
Sample 1 (2)

Sample 1

Full pattern degree of fit:	0.1500	
Mineral	Weight Percent	Normalized Results
NON-CLAYS		
Quartz	29.8	38.7
Kspar (intermediate microcline)	10.1	13.1
Dolomite	4.9	6.4
Total non-clays	44.9	58.2
CLAYS		
Illite (1M; R>3; 95%I)	13.6	17.6
Illite (R>1, 70-80%I)	7.6	9.9
Muscovite (2M1)	11.0	14.2
Total clays	32.2	41.8
TOTAL	77.0	100.0

Sample 1 Normalized

Legend:
- QUARTZ
- INTERMEDIATE MICROCLINE
- DOLOMITE
- ILLITE (1M; R>3; 5% exp)
- ILLITE (1M; 30% exp; R>1)
- MUSCOVITE (2M1)

Red is calculated, blue is measured, purple is auto background correction

Legend:
- Corundum
- QUARTZ
- INTERMEDIATE MICROCLINE
- DOLOMITE
- ILLITE (1M; R>3; 5% exp)
- ILLITE (1M; 30% exp; R>1)
- MUSCOVITE (2M1)
- 0
- 0
- 0
- 0
- 0

Red is calculated, blue is measured, purple is auto background correction

Legend:
- Corundum
- DOLOMITE
- MUSCOVITE (2M1)
- 0
- QUARTZ
- ILLITE (1M; R>3; 5% exp)
- 0
- 0
- INTERMEDIATE MICROCLINE
- ILLITE (1M; 30% exp; R>1)
- 0
- 0

Axis labels: Counts (y-axis), Two-Theta (x-axis)
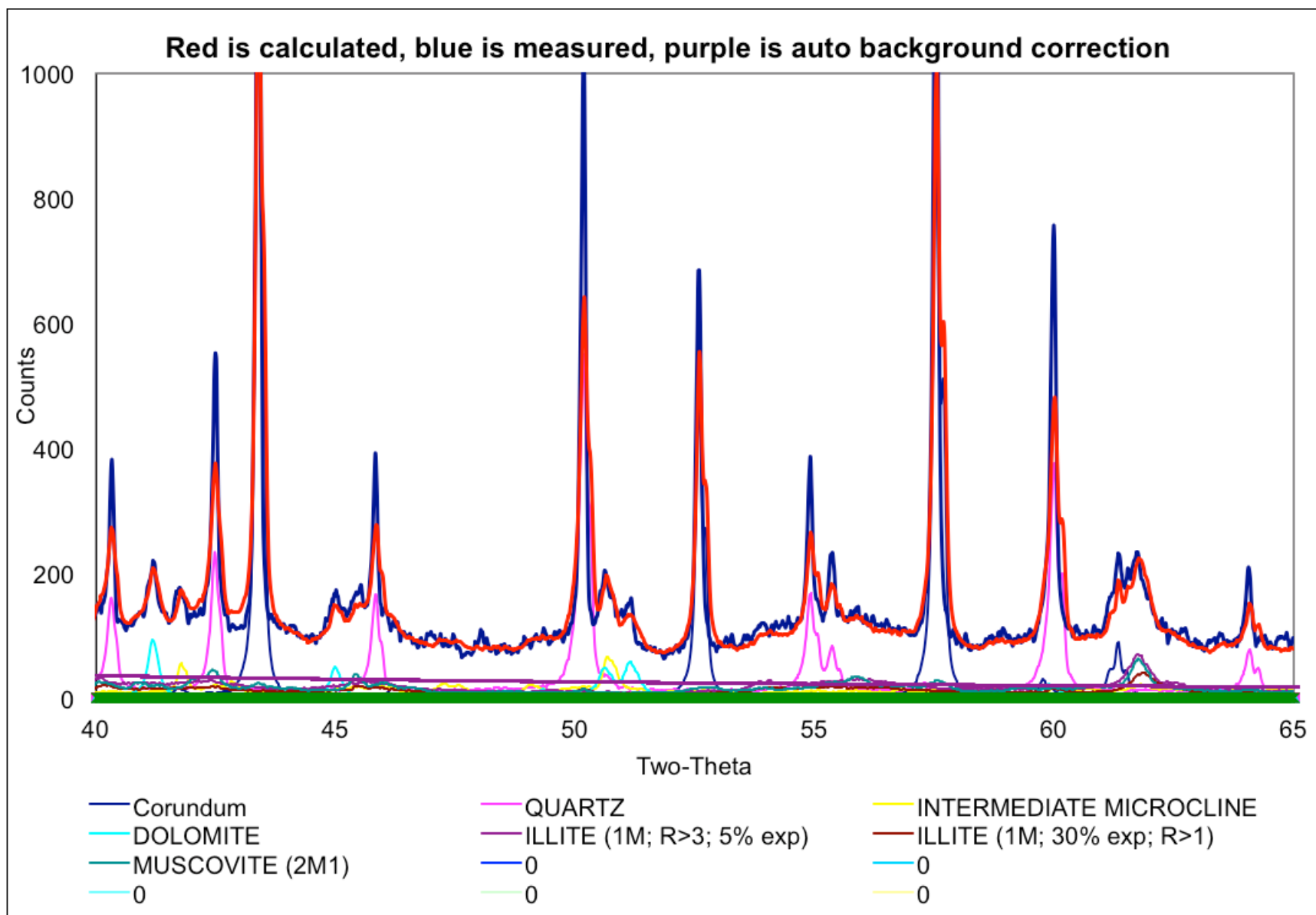
Sample 2 (4)

Sample 2

Full pattern degree of fit:	0.1837	
Mineral	Weight Percent	Normalized results
NON-CLAYS		
Quartz	41.3	59.9
Kspar (intermediate microcline)	8.6	12.5
Calcite	3.8	5.5
Total non-clays	53.8	77.9
CLAYS		
Smectite (ferruginous)	0.1	0.1
Illite (1M; R>3; 95%I)	10.6	15.4
Illite (R>1, 70-80%I)	4.6	6.7
Total clays	15.2	22.1
TOTAL	69.0	100.0
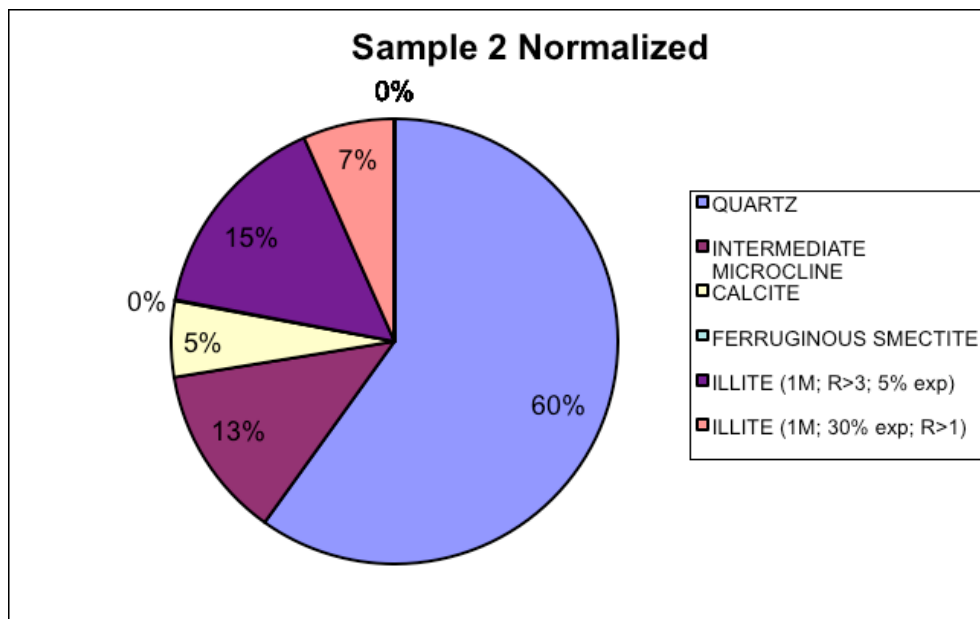
Sample 2 Normalized

Red is calculated, blue is measured, purple is auto background correction

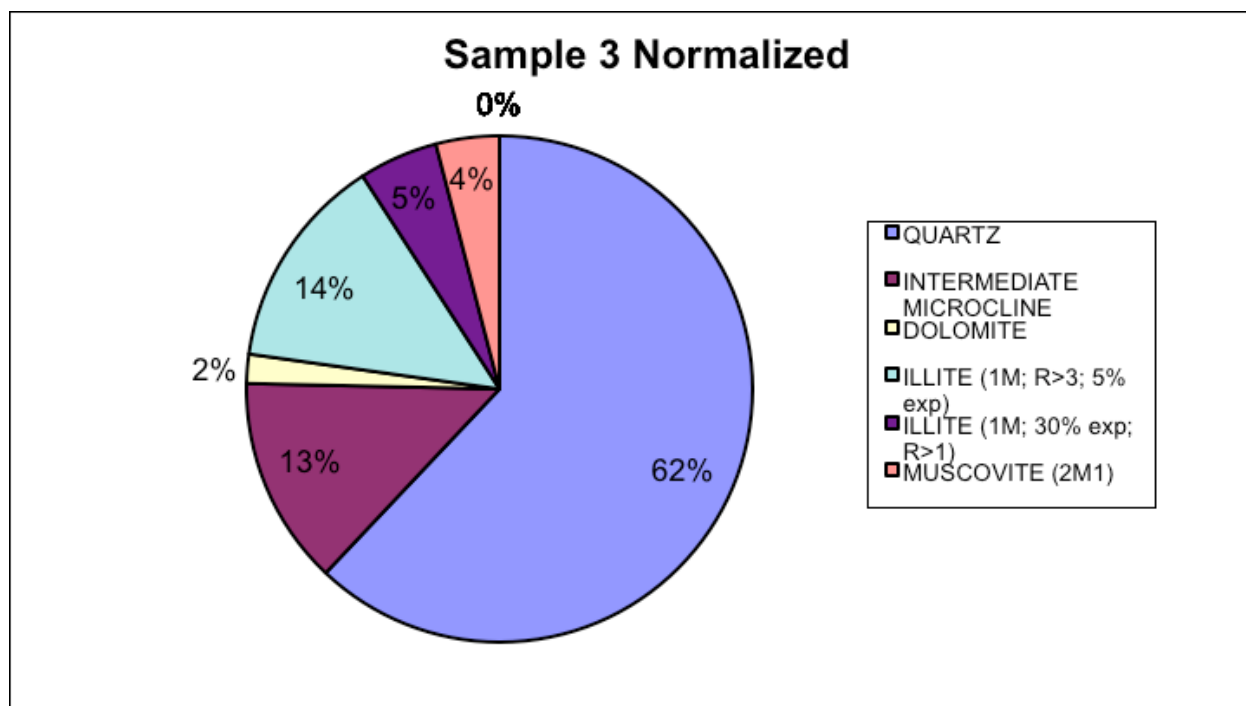Red is calculated, blue is measured, purple is auto background correction
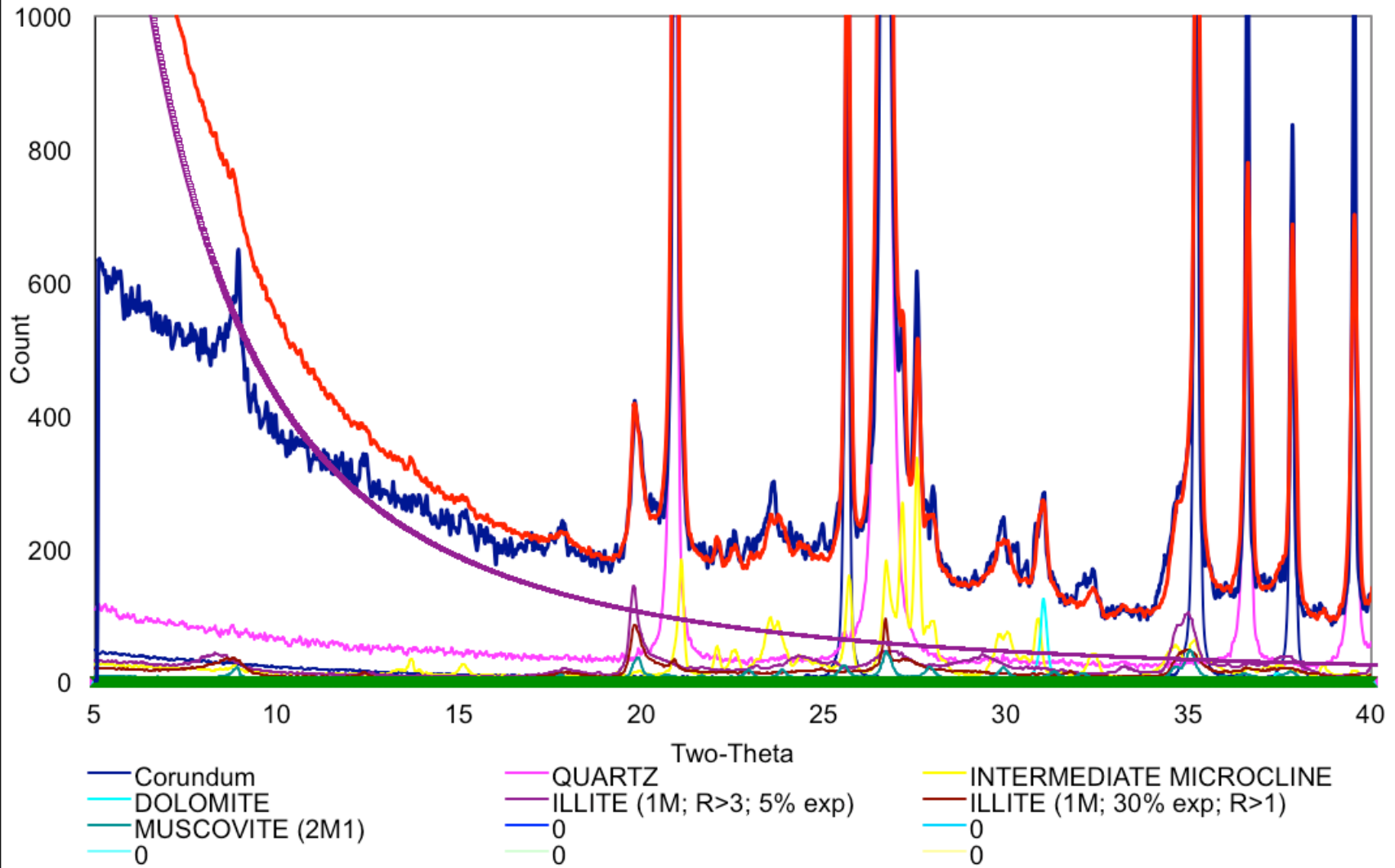
49
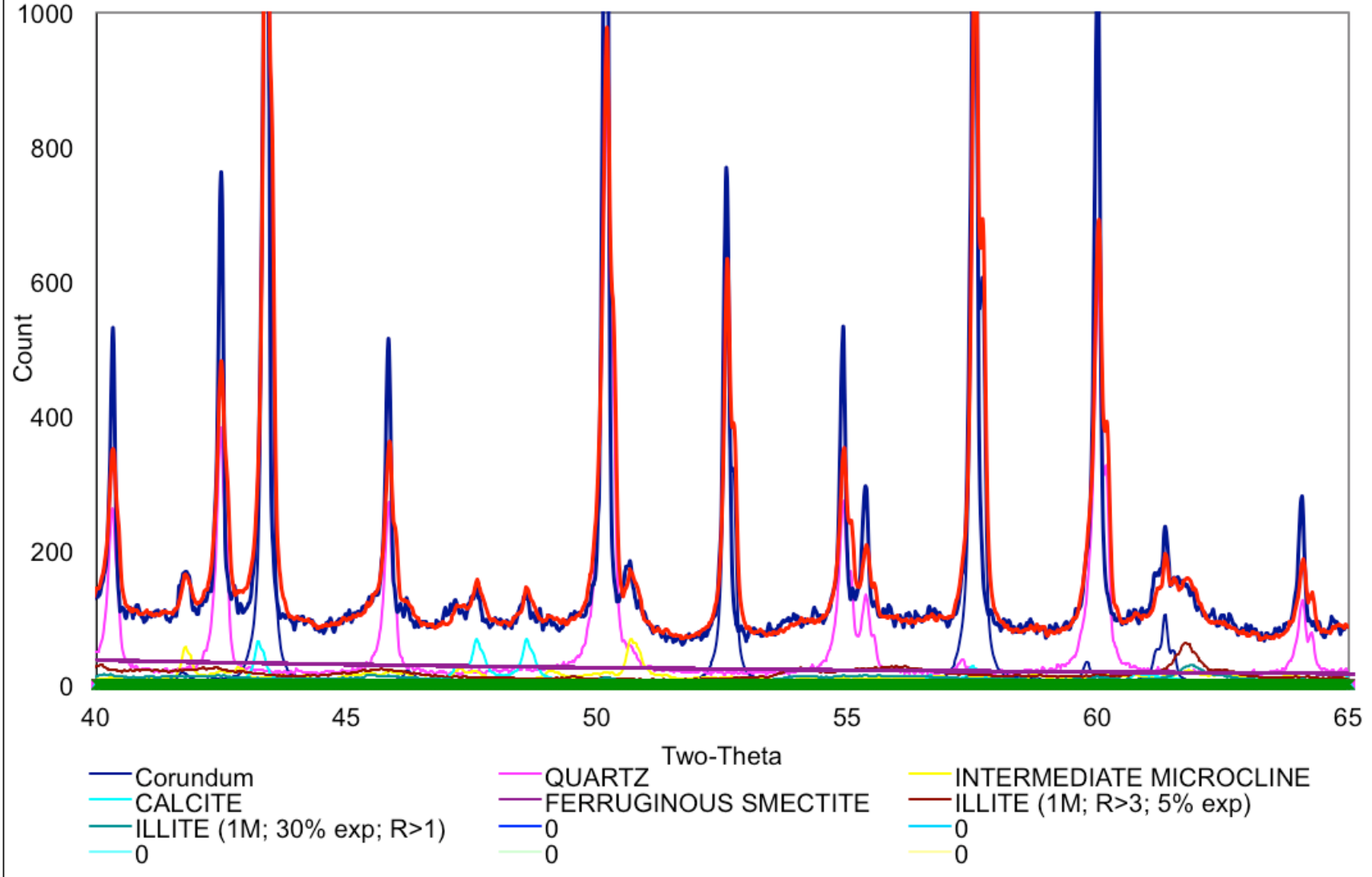
Sample 3 (HS2)

Sample 3

Mineral	Weight Percent	Normalized results
Full pattern degree of fit:	0.2068	
NON-CLAYS		
Quartz	48.7	62.1
Kspar (intermediate microcline)	10.4	13.3
Dolomite	1.5	1.9
Total non-clays	60.6	77.2
CLAYS		
Illite (1M; R>3; 95%I)	10.7	13.7
Illite (R>1, 70-80%I)	4.0	5.0
Muscovite (2M1)	3.2	4.1
Total clays	17.9	22.8
TOTAL	78.4	100.0

Red is calculated, blue is measured, purple is auto background correction

Red is calculated, blue is measured, purple is auto background correction

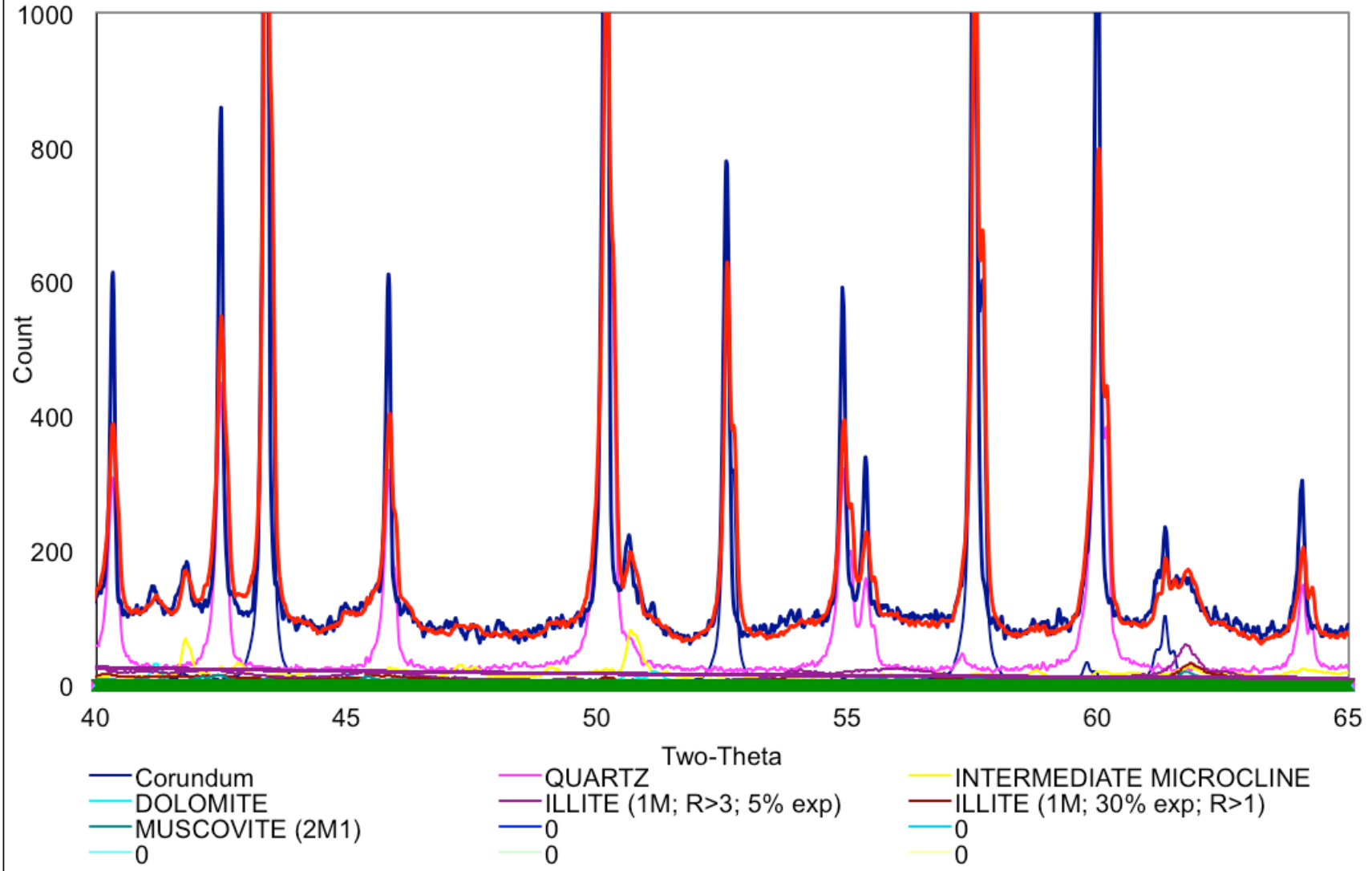*Sample Averages*

Sample Averages

Full pattern degree of fit:	0.1802	
Mineral	Weight Percent	Normalized Results
NON-CLAYS		
Quartz	39.9	53.6
Kspar (intermediate microcline)	9.7	13.0
Calcite	1.3	1.8
Dolomite	2.1	2.8
Total non-clays	53.1	71.1
CLAYS		
Smectite (ferruginous)	0.0	0.0
Illite (1M; R>3; 95%I)	11.6	15.6
Illite (R>1, 70-80%I)	5.4	7.2
Muscovite (2M1)	4.7	6.1
Total clays	21.8	28.9
TOTAL	74.8	100.0